AD-A064 488 PENNSYLVANIA STATE UNIV UNIVERSITY PARK MATERIALS RE--ETC F/G 20/3
TARGETED BASIC STUDIES OF FERROELECTRIC AND FERROELASTIC MATERI--ETC(U)
DEC 78 L E CROSS, R E NEWNHAM, G R BARSCH N00014-78-C-0291

UNCLASSIFIED NL

/ OF /
AD
AO 64488

END
DATE
FILMED
4 -79
DDC

LEVEL II

12 SC

# TARGETED BASIC STUDIES OF FERROELECTRIC AND FERROELASTIC MATERIALS FOR PIEZOELECTRIC TRANSDUCER APPLICATIONS.

Period January 1, 1978 to December 31, 1978

(9) Rept. for 1 Jan-31 Dec 78

OFFICE OF NAVAL RESEARCH

Contract No. (15) N00014-78-C-0291



APPROVED FOR PUBLIC RELEASE— DISTRIBUTION UNLIMITED

Reproduction in whole or in part is permitted for any purpose of the United States Government

(10) L.E. Cross,
R.E. Newnham,
G.R. Barsch
J.V. Biggers

(11) 31 Dec 78

(12) 72 p.

MATERIALS RESEARCH LABORATORY

THE PENNSYLVANIA STATE UNIVERSITY

UNIVERSITY PARK, PENNSYLVANIA 16802

# TARGETED BASIC STUDIES OF FERROELECTRIC AND FERROELASTIC MATERIALS FOR PIEZOELECTRIC TRANSDUCER APPLICATIONS

Period January 1, 1978 to December 31, 1978

OFFICE OF NAVAL RESEARCH

Contract No. N00014-78-C-0291



L.E. Cross
R.E. Newnham
G.R. Barsch
J.V. Biggers

CONTENTS

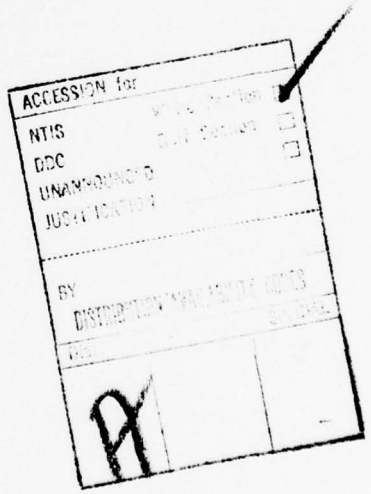

## ABSTRACT

This report documents work initiated during the first nine months of a major new five-year program which is focused on some of the fundamental problems in ferroelectric and ferroelastic crystals which are of special relevance to the design and development of new and improved materials for electromechanical transducers.

Electrostriction is the basic coupling mechanism between dielectric and mechanical properties in all present ceramic piezoelectric transducers, yet there is no adequate theoretical description of this phenomenon, and reliable experimental values are not available for the electrostriction constants of many simple insulators.

For experimental measurement of electrostrictive deformations an ultrasensitive AC dilatometer is being developed. The present instrument will resolve displacements of ~~$5.10^{-13}$ meters~~ (0.005Å) at 7.5 Hz, and is presently being used to measure electrostriction constants for a range of alkali halide crystals.

A comparative evaluation of lattice theoretical models previously used to explain the electrostriction constants in alkali halides shows the inadequacy of all current models and of the basic lattice dynamical framework used. In order to develop a more adequate approach the lattice theory of the elastic dielectric was begun for an anharmonic shell model, in which the nonlinearity of the electronic polarizability is included in a consistent manner in addition to the anharmonicity of the short-range overlap and of the coulomb forces. If successful for alkali halides, the theory will be applied to piezoelectric and ferroelectric prototypes of simple crystal structure.

For the important practical electrostrictor lead magnesium niobate (PMN) single crystals have been grown which are large enough to permit measurements of the electrostriction constants. A new digital program-controlled flux growth

system has been installed and is being used to grow single crystals of compositions in the $PbZrO_3$:$PbTiO_3$ solid solution family.

New replication techniques are being developed for the synthesis of ceramic: polymer composites with controlled interphase connectivity designed to optimize the properties for piezoelectric voltage mode applications. Synthesis techniques have also been developed to generate ferroelectric powders in the bismuth oxide layer structure compounds which have very marked shape anisotropy, so as to permit the fabrication of grain oriented piezoceramics without the expensive and time consuming step of uniaxial hot pressing.

Work has also been initiated on the growth of bicrystals of ferroelectric triglycine sulfate and of paraelectric potassium tantalate niobate to explore the interface phenomena at an artificial single grain boundary of controlled orientation. Both intergrown and diffusion bonded interfaces are under study.

ADAGE computer graphics techniques are being applied to the development of more comprehensive phenomenological descriptions of ferroelectricity in perovskite, tungsten, bronze and bismuth oxide layer structure compounds and solid solutions.

## 1. INTRODUCTION

This report describes work carried out over the period from April 1 to December 31 on ONR contract N00014-78-C-0291 which initiates a new five-year study of several of the more important basic and applied problems associated with the development of new and improved materials and new understanding of the basic phenomena which are important in piezoelectric transducer systems.

Of necessity, much of the time in this first nine months has been taken up assembling the people and equipment necessary for the new research topics which are being undertaken. In spite of this necessary focus, however, several important advances have been made.

For the experimental determination of electrostriction in simple low permittivity solids a new type of AC capacitance dilatometer was proposed. Over the past six months, this instrument has been designed, constructed, and is now being tested. The first results already demonstrate the soundness of the original design principles. The present sensitivity permits the resolution of a displacement amplitude of 0.005Å ($5.10^{-13}$ meters) at a frequency of 7.5 Hz, thus it is already very close to the design target, and adequate for the precise electrostriction measurements in many of the insulator crystals of most theoretical interest. A paper describing this instrument will be presented at the 32nd Annual Frequency Control Symposium in Atlantic City in June, 1979.

The theoretical studies of electrostriction are also well underway. Dr. Achar, working in close cooperation with Professor Barsch, has recalculated the electrostriction constants for alkali halides, using the three presently available theoretical models but with the most recent values of the input parameters. These calculations clearly exhibit the poor agreement from presently available theories, and confirm the disturbing feature that the more sophisticated models do not represent significant improvement over the earliest point charge treatments.

A feature of the earlier model treatments which is believed to be most important is the neglect of the shell polarizability in the shell models applied. The theory is now being reformulated to take this into account. Phenomenologically it is evident that in the systems which have been measured, low permittivity solids generally have higher $Q_{ijkl}$ constants and high permittivity solids have lower values, where the $Q_{ijkl}$ are the polarization related electrostriction constants. Since there is more than 2 orders of magnitude in the range of Q values, it is obviously very important to understand whether this coupling is fundamental. If higher K materials could be found which have very high $Q_{ijkl}$ values, their application would make a major improvement in transducers.

Work on two-phase ceramic:plastic and ceramic:ceramic composites is being carried forward on two parallel approaches. Dr. Brendan Hardiman, who has joined the group from A.G. Telefunken Laboratories, is exploring new techniques for replicating 3:1 connected ceramic:plastic composites in which the scale of the macrostructure can be tailored over a very wide range. The method uses a lost-wax casting process, but now with a reusable template which can be controlled very precisely. In an alternative strategy, we are exploring extrusion techniques for making ultrathin PZT rods (100 to 200 μmeters) which can then be fabricated in the flexible green state into many of the complex interconnected structures required.

The study of grain oriented ceramics has focused on the task of generating fine powders of the bismuth oxide layer structure compositions which have very marked shape anisotropy. By reacting the mixed oxides in a eutectic KCl:NaCl salt bath, we have found that $Bi_4Ti_3O_{12}$ and $Bi_2WO_6$ can be produced as a micron-sized powder with very marked platey character. Thus without the expense of the uniaxial hot pressing:hot extrusion techniques which are being used in Japan we can produce well oriented grain texture.

To permit better control in the crystal growth studies, a new digital μ data track temperature programming system has been installed on the flux growth furnace. Crystals of $Pb_3MgNb_2O_9$ suitable for the measurement of the single crystal electrostriction parameters have been grown, and work is now progressing on the growth of crystals in the PZT solid solution family.

Studies of the "model grain boundary" have been initiated using water-soluble triglycine sulfate and paraelectric KTN as the material systems. Bi-crystals of TGS have been produced which show limited areas of good bonding, and the directions for improving the technique are being explored. A miniature hot-pressing rig has been built for controlled diffusion bonding of inorganic ferroelectrics. Preliminary tests on quartz crystals have shown the possibility of producing good high-strength bonding.

The thermodynamic phenomenology for pure lead zirconate:lead titanate solid solutions developed under ONR contract N00014-76-C-0515 was taken on that program to the stage where the full set of constants up to sixth rank in the Devonshire formalism had been evaluated for all single cell compositions, and gave a coherent and unified description of the dielectric, elastic, and thermal properties.

On this program, similar methods using the ADAGE graphics system are being extended to the practical doped PZTs, and the PLZT family. The programs are also being reformulated to the 4/mmm prototype symmetry so as to be able to describe the very large families of tungsten bronze and bismuth oxide layer structure ferroelectrics.

# 2. ELECTROSTRICTION

## 2.1 Introduction

There is probably little need to reiterate at this stage the very basic importance of electrostriction to electromechanical systems. For all ferroelectrics derived from centric prototypes, a group which includes all present generation piezoceramics, the single domain piezoelectric constants can be directly traced to electrostriction of the prototype. Even the domain and phase boundary contributions to strain in the more complex ceramics can be traced back to what are basically electrostrictive deformations, yet we have no viable theoretical description of electrostriction even in simple solids and almost no reliable experimental values on which to base such theories.

To rectify this deplorable situation, a two-pronged attack is clearly necessary. First, the background of reliable experimental values for electrostriction constants of simple solids must be built up, and second the theoretical framework must be established to give a properly based atomistic description of the phenomenon.

In the experimental area we proposed to set up to measure electrostriction both by the direct method (measuring the change of sample dimensions under E field) and by the converse method (studying the change of dielectric permittivity under mechanical stress). Over the past six months, emphasis has been on developing the exceedingly sensitive AC dilatometer required for the direct study of electrostrictive deformation.

The theoretical approach has been first to reexamine the earlier theories of Grindlay and Wong (1969), of Srinivasan and Srinivasan (1972) and of Goyal et al. (1977) for electrostriction in the alkali halides. To recalculate for representative crystals on each theory using a common most recent set of input

parameters so as to be able to compare properly these earlier studies. Unfortunately, this work has shown that agreement between theory and experiment is not radically improved, nor are the more recent sophisticated theories any significant improvement over the earliest simple point charge model.

## 2.2 Development of the Experimental Technique for Direct Measurement of Electrostriction in Simple Solids

### 2.2.1 Design of the AC Dilatometer

The dilatometer proposed was based on a design by Bohaty and Haussühl(1977) for an AC capacitor type dilatometer (Fig. 2.1). In their system the electrostrictive crystal of interest (a) cut and oriented in the correct manner and plated with evaporated metal electrodes is mechanically connected through an insulating perspex support to the upper plate of the strain sensing capacitor (b). A standard piezoelectric crystal (d) is electroded and mounted in a manner so that the piezoelectrically generated strain is communicated in a similar manner to the lower plate of the strain sensing capacitor (c). If crystal (a) is driven with a large AC voltage at a frequency of 80 Hz, plate (b) will be excited mechanically with a component of its motion at 160 Hz (2 $\omega$) through the electrostrictive strain generated in (a) which will be proportional to $V^2$. Crystal (d), the piezoelectric standard, is driven through a frequency doubling circuit phase locked to the generator supplying (a). The piezoelectric strain in (d) will also modulate the position of the lower plate (c) of the sensing capacitor at a frequency of 160 Hz, in phase with the vibration of plate (b) generated by crystal (a). When the phase and amplitudes of the fields at (a) and (d) are suitably chosen, the two plates (b) and (c) will vibrate in exact synchronism producing a net zero modulation of the separation and thus of the capacitance of bc at 160 Hz.

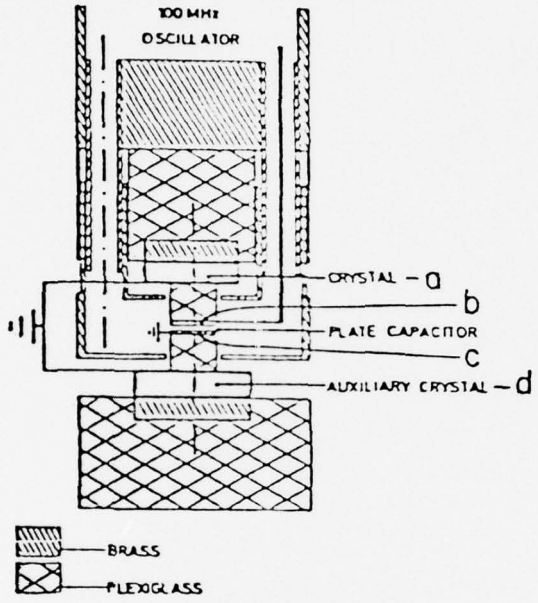


Fig. 2.1 AC differential dilatometer for measuring electrostrictive coefficients after Bohatý and Haussühl, 1977.

Clearly, if this null condition can be precisely established, from the AC voltage applied to the standard piezoid (d) and its known dimensions, the amplitude of the strain at c can be calculated. Since this must at null be exactly the same as the 160 Hz strain at (b) and the voltage applied to (a) is known, the appropriate electrostriction constant for (a) can now be calculated. To sense the null condition in the capacitor bc, the capacitor is used as the tuning element of a 100 MHz oscillator, detecting the modulation of bc by a discriminator and phase locked detector locked to the 160 Hz driving oscillator.

In the system which we have designed and constructed, the mode of sensing the capacitance is different, and is, we believe, a radical improvement over the Band H design. For a simple parallel plate capacitor dilatometer operating in dry nitrogen the sensing capacitance C is given by

$$C = \varepsilon_o \frac{\varepsilon A}{\ell}$$

where $\varepsilon_o$ is the permittivity of free space, $\varepsilon$ the permittivity of dry nitrogen at atmospheric pressure, A the plate area, and $\ell$ the separation. The capacitance change $\Delta C$ associated with a small change in $\ell$ ($\Delta\ell$) will be given by

$$\Delta C = \left(-\frac{\varepsilon_o \varepsilon A}{\ell^2}\right)\Delta\ell = K\Delta\ell$$

Obviously the sensitivity constant K can be made very large if $\ell$ can be made very small. In a practical system, however, a limiting value of $\ell$ is set by slow dimension changes due to thermal drift, and capacitance changes associated with gas pressure changes, which can take $C_o$ outside the linear range of any very high sensitivity discriminator. In the AC dilatometer, however, since only the component of the plate separation $\Delta\ell(2\omega)$ at the piezoelectric drive frequency is of interest, a DC servo, actuated by an error signal from the static capacitance value can be used to stabilize $C_o$.

A simple block diagram of the full measuring system is given in Fig. 2.2. The components of the mechanical circuit inside the dotted box (a,b,c,d) are identical in principle to those used by B and H. However, to sense and control the capacitor bc a General Radio 1620 capacitance measuring assembly is used (j,k,l).

To obtain maximum sensitivity, the bridge is operated at a frequency of 1 KHz, the standard piezoelectric crystal is driven at 7.5 Hz and the electrostrictor under study at 3.75 Hz. In the 1620 assembly the type 1238 detector (ℓ) provides synchronous detection of both the in-phase and the quadrature components of the bridge unbalance signal, phase locked to the 1316 bridge driving oscillator (K). The in-phase DC signal output is used to drive a Burleigh RC42 Servo amplifier which actuates three parallel piezoceramic mechanical actuators controlling the static plate separation (bc).

A second phase locked detector (n) (Keithley Model 822 with 821 phase shifter) also looks at the in-phase unbalance signal but now with a time constant $\tau \ll 0.1$ seconds. The output of this detector is passed to a Princeton HR8 lock-in amplifier which is phase locked to the 7.5 Hz slave oscillator driving the standard piezoelectric crystal.

The DC output of this lock-in provides the null detector which senses the condition under which the plates b and c are being driven in phase at the same amplitude, i.e. that the separation bc contains no component in phase with the driving oscillators (a) and (d).

### 2.2.2 Construction of the Dilatometer

The mechanical system is built around a Burleigh Model RC 110 1R Fabry-Perot Interferometer. The IR interferometer already incorporates PZT piezoelectric drivers which actuate the movable interferometer plate mount to provide 8 μmeters of linear movement and 3.5 μm alignment tilt. This mechanical

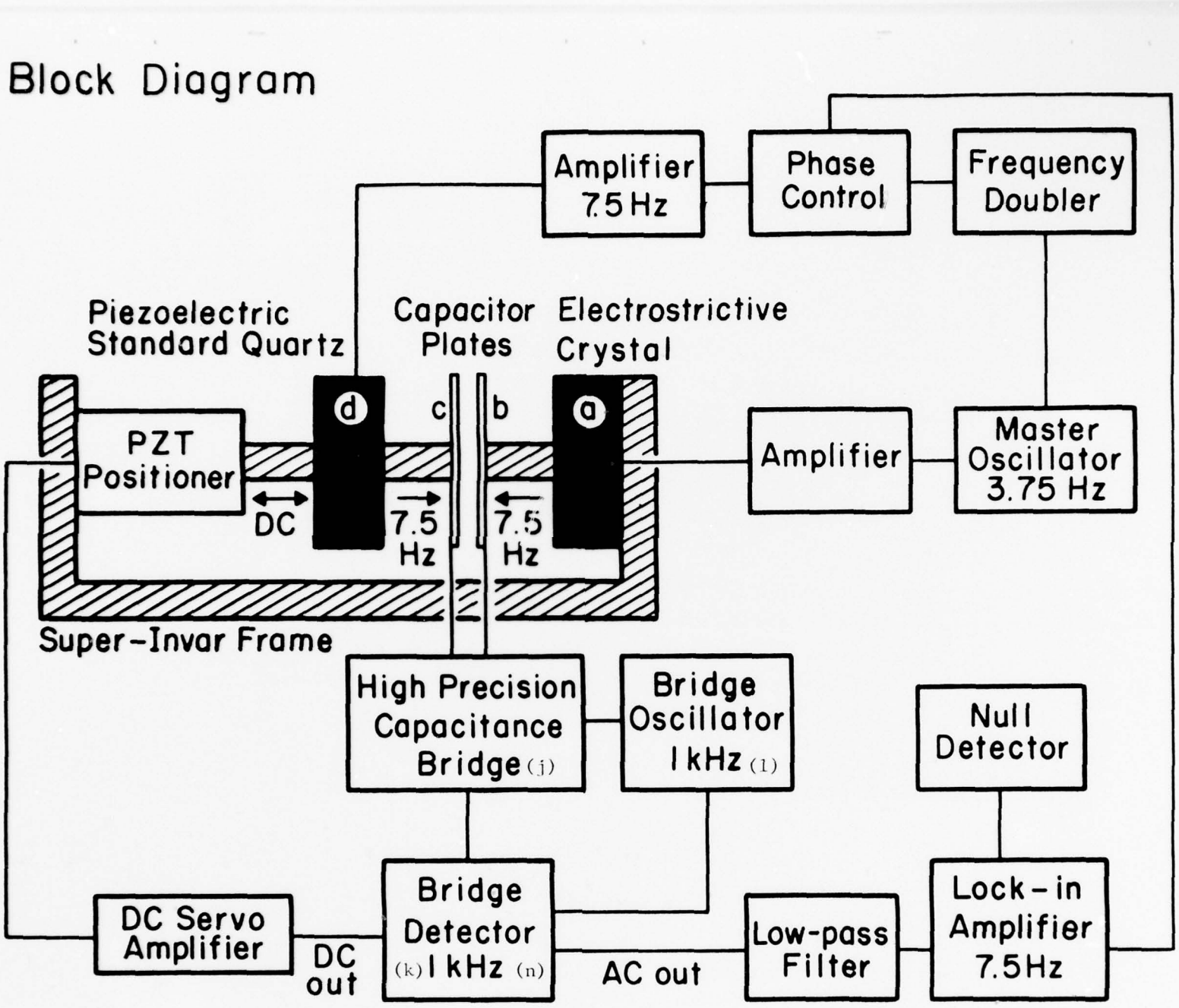


Fig. 2.2 Schematic diagram of the AC dilatometer.

frame (Fig.2.3) is constructed from super invar ($\alpha \leq 0.36 \times 10^{-6}/°C$) and provides a 0 - 150 mm cavity into which to mount the two driver crystals and the sensing capacitor with all tilt and alignment adjustments already built in.

The elaton frame fits within a model RC 75 temperature control chamber which stabilizes the structure to $< 0.05°C$.

The arrangement of the driver generators and sensing capacitor is shown schematically in Fig. 2.4. The standard piezoelectric crystal is a large X cut quartz plate mounted between lucite supports (Section a).

The sensing capacitor plates are of fused silica, with sputtered gold surfaces (b) and the electrostriction section c which contains the electrostrictive plate under study is a similar sandwich structure. In this section the perspex insulator on the live side of the electrostrictor crystal is made very thick so that the field across this section is low and the electrostriction of the perspex does not contribute to the total linear deformation. Each section of the assembly is separately electrostatically screened, and all connections are through coaxial cables.

Both the standard quartz driver and the electrostriction crystal are held in place by a very thin film of Eastman 910 cyanoacrylate ester cement.

The Burleigh RC 75 thermal enclosure which houses all mechanical components is mounted on a EPOI vibration isolation platform, which is itself supported on an air mounted granite slab (Fig. 2.5).

### 2.2.3 Dilatometer Performance

One advantageous feature of the present design of AC dilatometer is that the performance can be verified stage by stage. First the drift correction of the DC Servo can be checked.

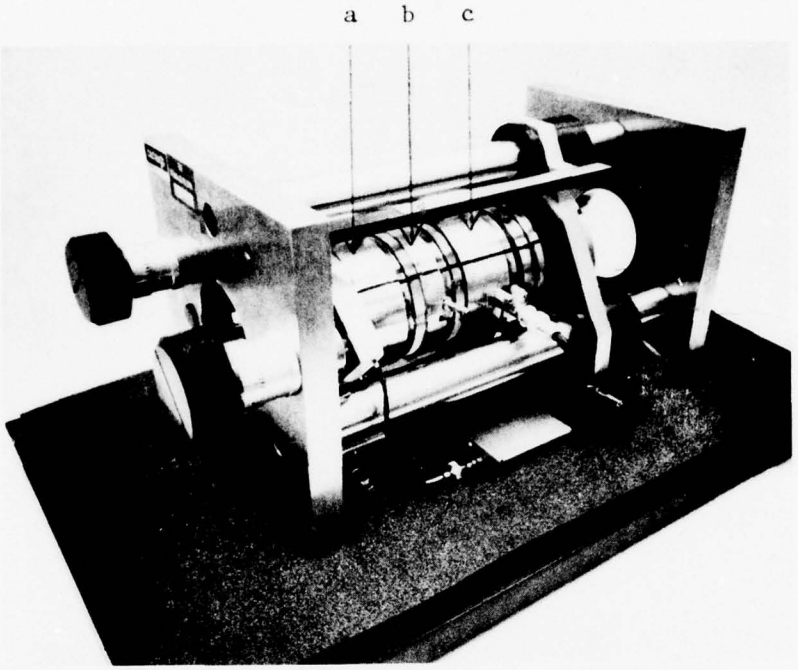


Fig. 2.3 Burleigh Model RC 110 I.R. Fabry Perot cavity with AC dilatometer sections in place.

(a) Standard piezoelectric driver.
(b) Shielded dilatometer capacitor.
(c) Electrostriction driver section.

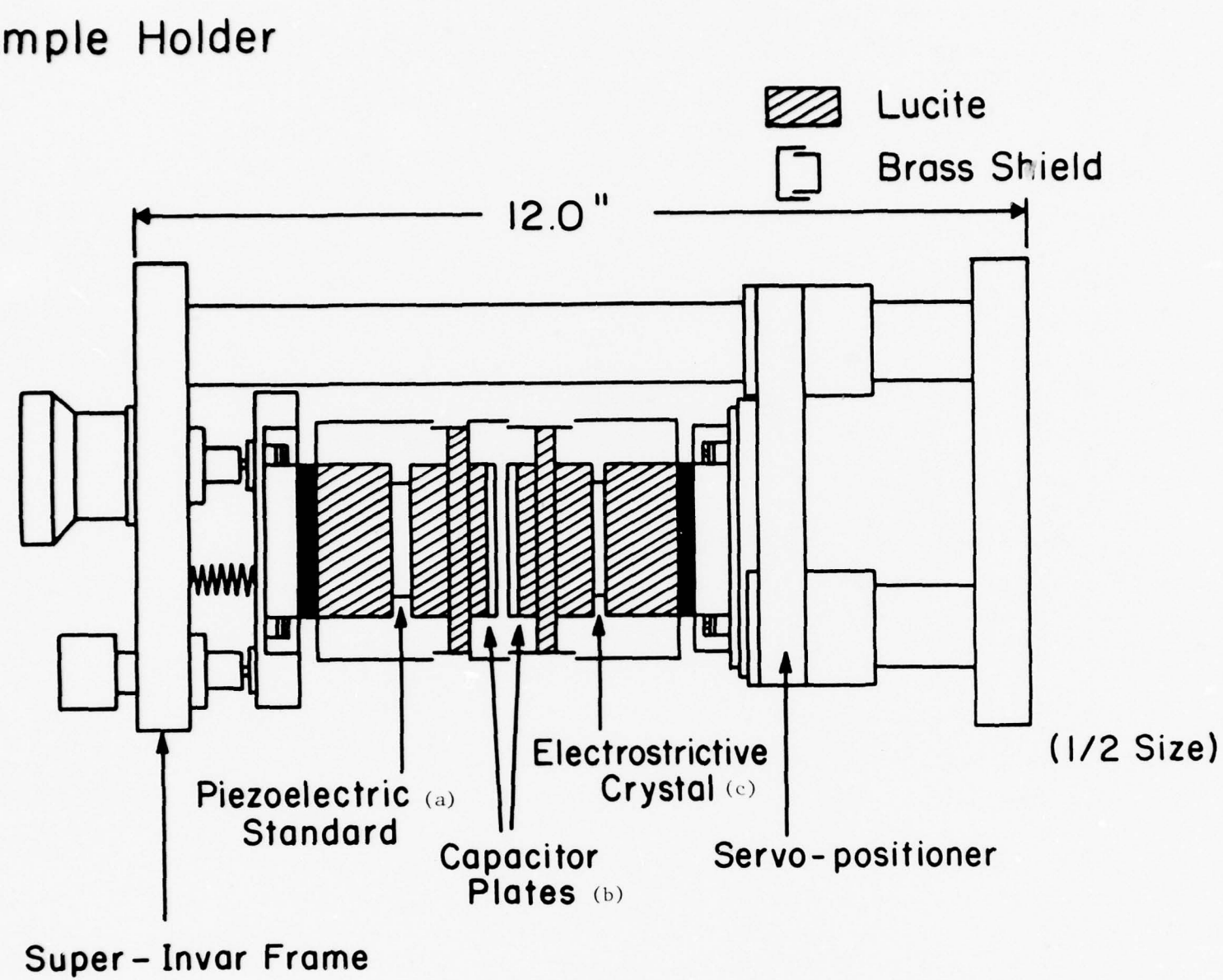


Fig. 2.4 Schematic of the dilatometer and support structure.

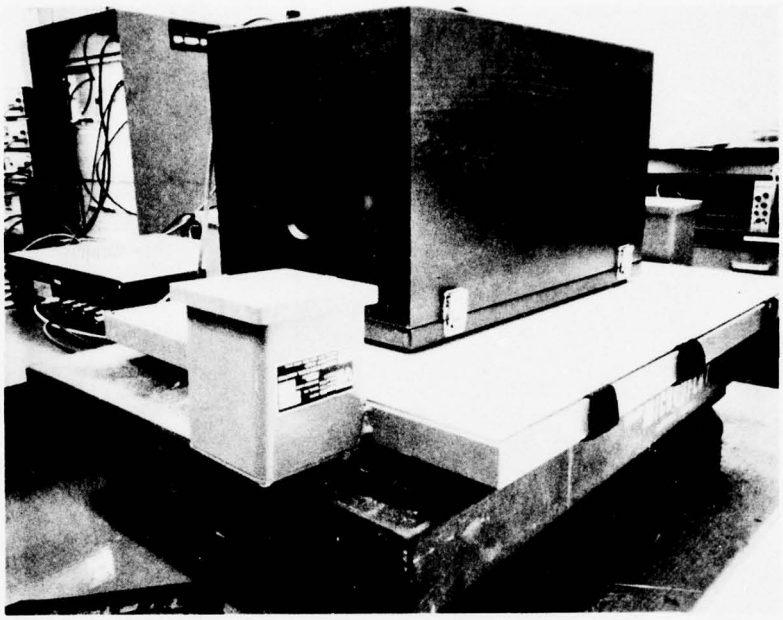

Fig. 2.5 Mounting arrangement for the AC dilatometer housed in the Burleigh RC 75 temperature controlled enclosure.

After the system has stabilized for some 4 hours, the DC Servo system is disabled and the intrinsic drift rate of the capacitance determined by measuring the bridge unbalance signal as a function of time (Fig. 2.6). By rebalancing the bridge periodically the capacitance increment for a given unbalance voltage can be determined, and from the $\Delta C$ a corresponding $\Delta \ell$ can be calculated.

It is evident from Fig. 2.6 that without compensation the drift rate corresponds to a plate separation change of 1Å/minute. Maintaining the same conditions, the DC Servo is now turned on, and at the same gain setting no drift is discernible at all. Turning the gain up by a factor of 100, however (Fig. 2.6 right-hand scale), it is evident that the drift rate has been decreased by a factor $\sim 2 \times 10^{-3}$ and now corresponds to a linear dimension change $\sim .002$Å/minute.

Thus the detector amplifier can be maintained at 110 dB over long periods of time without drifting out of the linear range of the amplifier.

To check the AC sensitivity the standard quartz crystal was driven by a Wavetek Model 142 oscillator at 7.45 Hz. The conditions recorded in Table 2.1 were set up.

With 20 volts RMS applied to the bridge, the lock-in output as a function of voltage applied to the quartz crystal is given in Fig. 2.7. The linear relation expected for a piezoelectric is clearly evident. Taking a value of $d_{11} = +2.3.10^{-10}$ and a resolution limit of ±0.2 mV gives for the smallest resolvable increment $\Delta \ell = \pm 5.10^{-3}$Å.

As a further check of the system, the lock-in output for a fixed value of drive voltage to the quartz (10.8 V RMS) was recorded as a function of voltage applied to the bridge. If the measured signal comes only from the bridge unbalance, this should scale linearly with the applied voltage as is evident in Fig. 2.8.

Experiments are now in progress to test the electrostrictive cell which is the final component in the system.

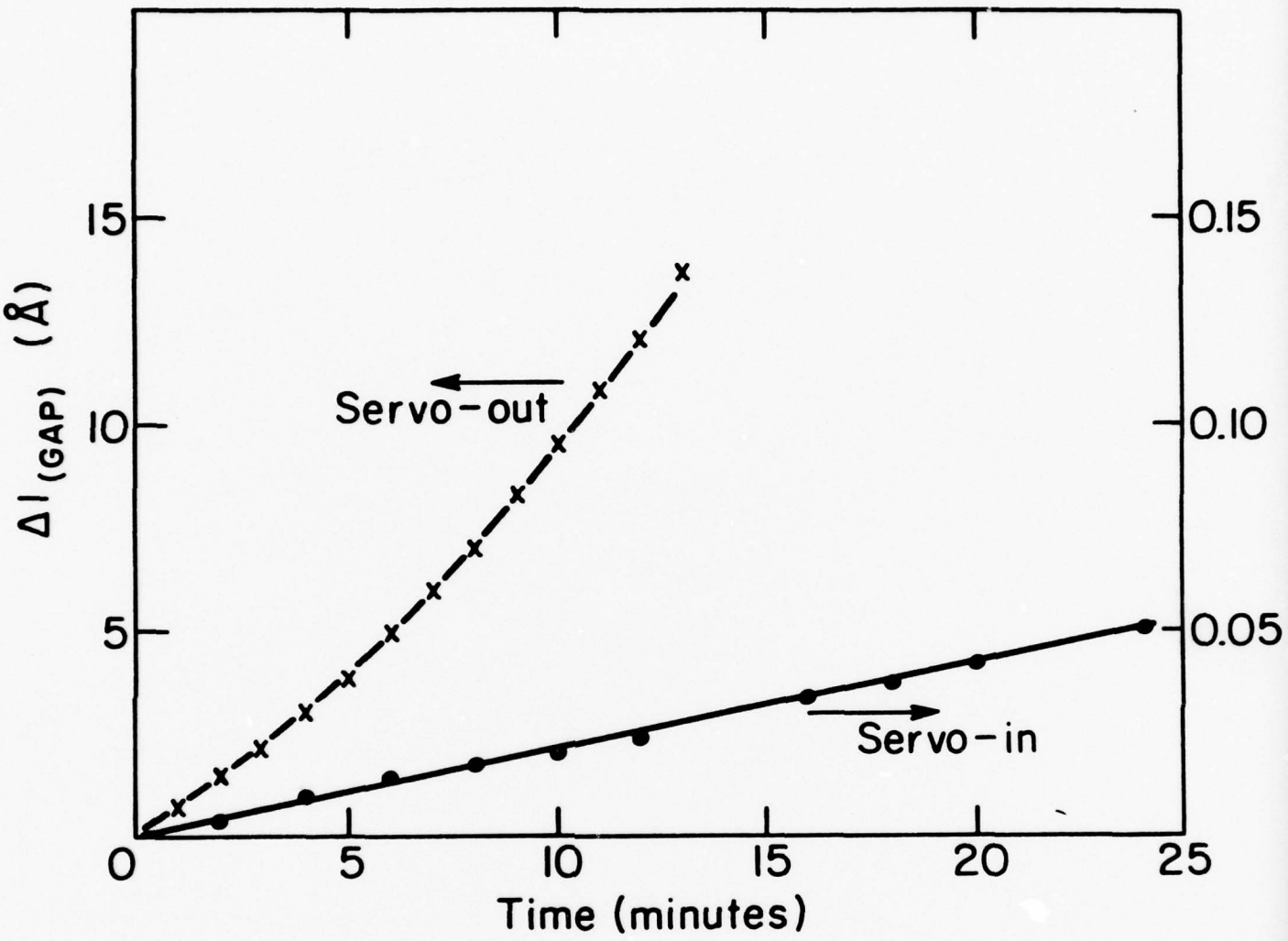


Fig. 2.6 DC plate separation change $\Delta\ell$ as a function of time with and without the drift compensation Servo amplifier.

Table 2.1 Conditions used in the determination of AC sensitivity

| | | |
|---|---|---|
| 1. | Temperature | 29.4 ± 0.04°C |
| 2. | Capacitance Bridge: | 1 kHz, 20-30 Vrms |
| | Gain | 80-100 dB |
| | Capacitance | 250 pF (plate gap 70 μm) |
| | Conductance | $1.4 \times 10^{-4}$ μ℧ |
| 3. | Quartz Driving: | 7.45 Hz, 0-10 Vrms |
| 4. | Band Pass Filter: | 2.5 - 13 Hz |
| 5. | Lock-in Amplifier: | |
| | Signal Channel | 7.45 Hz |
| | Mode | Band Pass |
| | Q | 100 |
| | Time Const. | 10 sec |
| | Reference Channel | |
| | PSD | Normal |

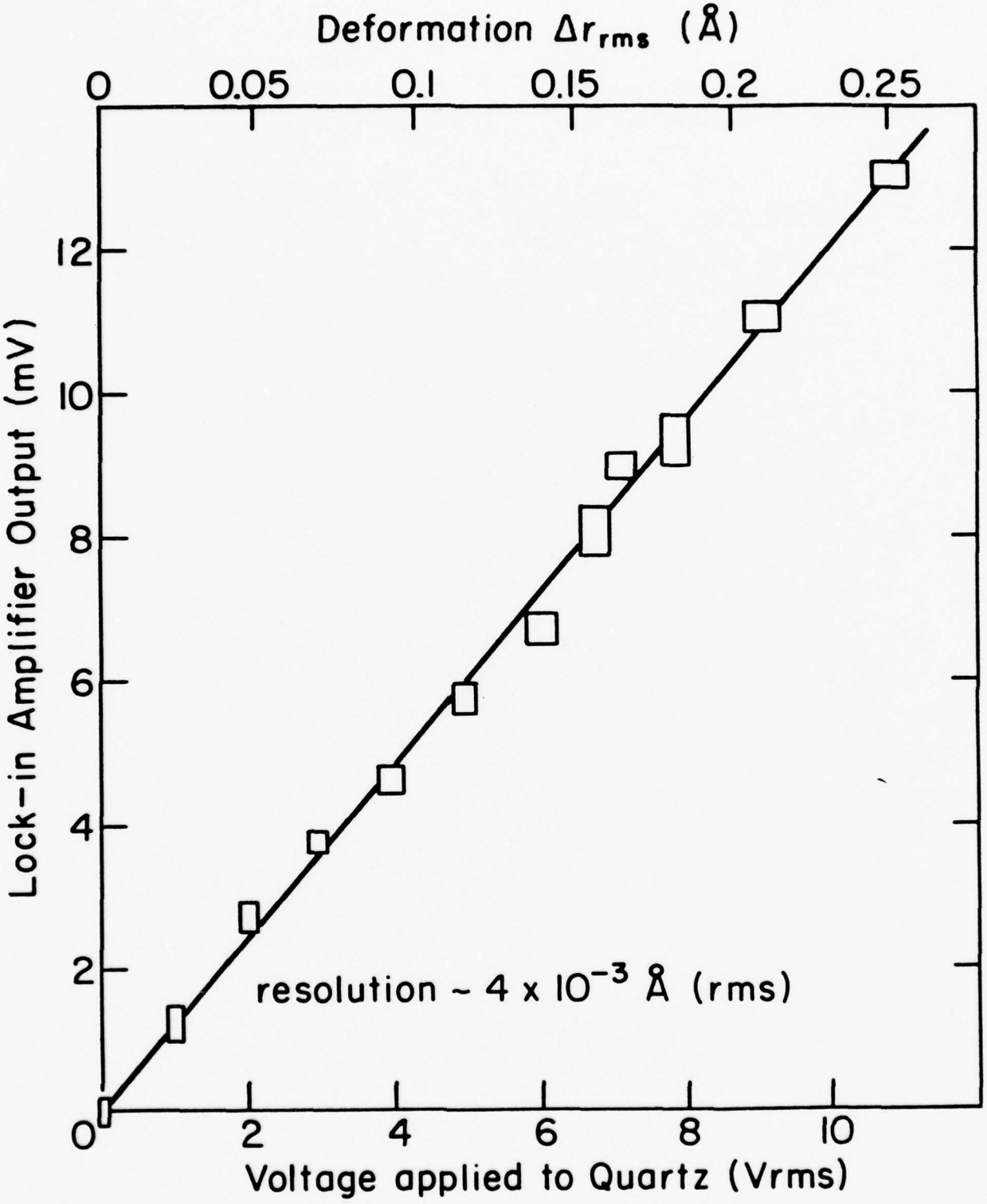


Fig. 2.7 Dilatometer output as a function of driving voltage applied to the quartz standard crystal and of equivalent AC displacement amplitude.

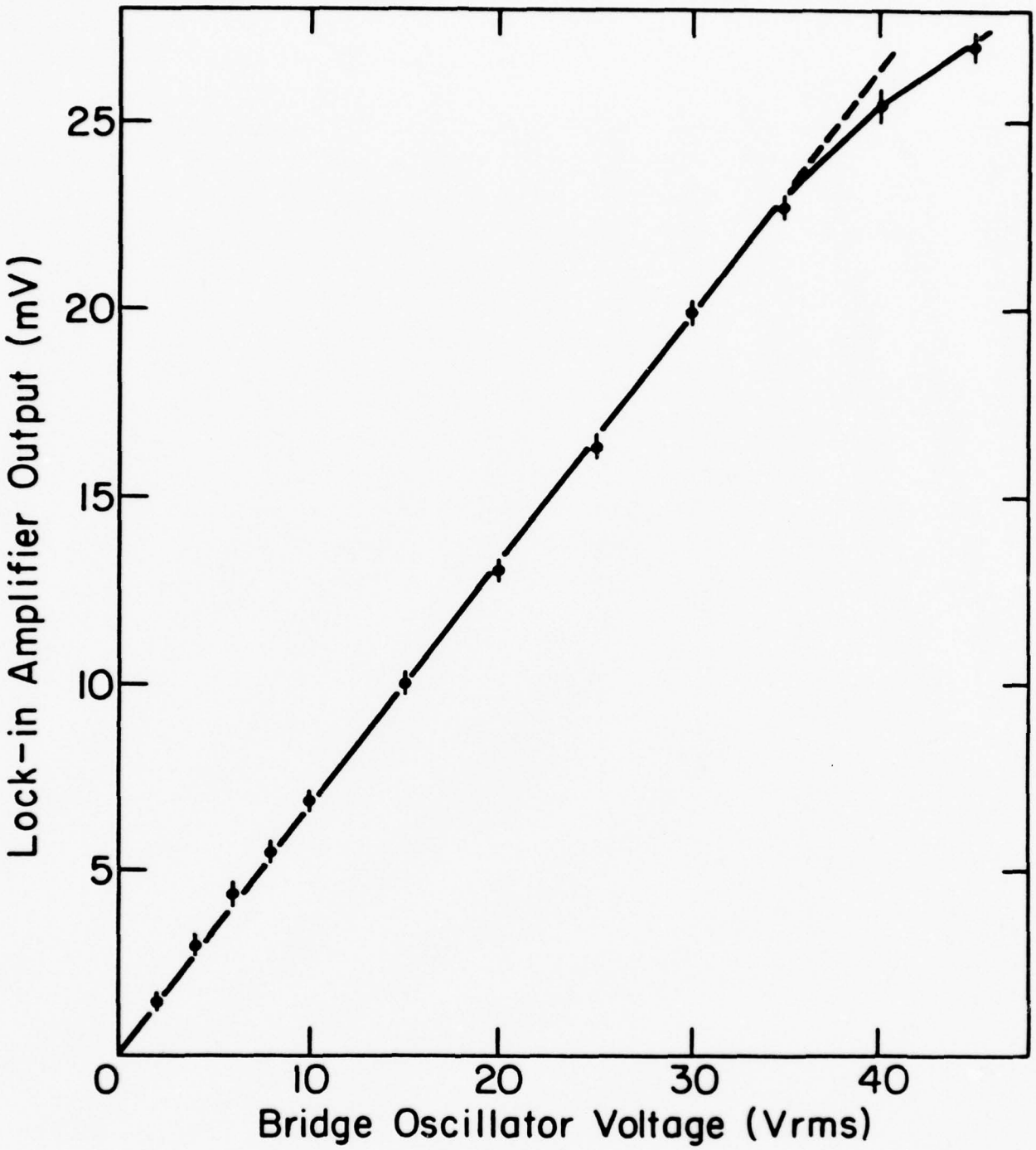


Fig. 2.8 Dilatometer output as a function of bridge oscillator voltage for fixed 10.8 V rms applied to the quartz crystal.

## 2.3 Lattice Theory of Electrostriction

### 2.3.1 Technical Problem

As shown phenomenologically the piezoelectric constants of ferroelectrics derived from centric prototypes (the case for all present piezoceramics) are proportional to the electrostriction constants and the spontaneous polarization. Thus for systematic attempts to find new materials with larger electromechanical coupling factors the microscopic parameters which determine these properties must be well understood. A critical analysis of previous theoretical treatments of electrostriction shows that all are inadequate even for such simple solids as alkali halides. The purpose of the present work is to develop a more adequate theory of electrostriction, to apply it to alkali halides and, if successful, to selected piezoelectric and ferroelectric materials occurring in simple structures. It is hoped that the results will provide heuristic guidelines for maximizing the electrostriction constants for a given crystal structure.

### 2.3.2 Methodological Approach

All previous theories of electrostriction are based either on the rigid ion model, or on various versions of the shell model of lattice dynamics. Obviously, the rigid ion model is inadequate because electronic polarizability is neglected altogether. In the available shell model treatments electronic polarizability is only included in the harmonic approximation, in which the strain dependence of the electronic polarizability is neglected. In addition, other simplifying assumptions of dubious validity are made.

The present work consists of two phases. In the first phase several anharmonic shell models are being investigated in a rigorous and consistent manner. Promising models which can satisfactorily account for electrostriction in alkali halides will be subsequently applied to piezoelectric and ferroelectric materials occurring in simple crystal structures. For the second

phase empirical pseudopotential calculations in conjunction with the dielectric screening approach are envisaged which would relate the empirical parameters in the anharmonic shell models to more basic microscopic physical quantities.

2.3.3 Technical Results

2.3.3.1 Definition of Electrostriction Constants

Of the various free energy functions pertaining to the elastic dielectric we choose the Helmholtz free energy $F(T,\eta_{ij},E_k)$ as a function of temperature T, strain $\eta_{ij}$, and electric field $E_k$ (i,j,k=1,2,3). The electrostrictive constants are defined as the third derivative of the free energy according to

$$2f_{ijkl} = \left(\frac{\partial^3 F}{\partial\eta_{ij}\partial E_k\partial E_\ell}\right)_T \tag{2.1}$$

with the definitions for the stress tensor

$$\sigma_{ij} = \left(\frac{\partial F}{\partial\eta_{ij}}\right)_{T,E_k} \tag{2.2a}$$

and of the dielectric constant tensor

$$\varepsilon_{k\ell} = \left(\frac{\partial D_k}{\partial E_\ell}\right)_{T,\eta_{ij}} = -\left(\frac{\partial^2 F}{\partial E_k\partial E_\ell}\right)_{T,\eta_{ij}} \tag{2.2b}$$

one obtains from equ (2.1) after reversing the sequence of the derivatives the alternative expression

$$2f_{ijkl} = \left(\frac{\partial^2\sigma_{ij}}{\partial E_k\partial E_\ell}\right)_{T,\eta_{mn}} = -\left(\frac{\partial\varepsilon_{k\ell}}{\partial\eta_{ij}}\right)_{T,E_m} \tag{2.3}$$

The electrostrictive constants have the symmetry properties

$$f_{ijkl} = f_{jikl} = f_{ijlk} = f_{klij} \tag{2.4}$$

According to equ (2.3) the electrostrictive constants $f_{ijkl}$ are the first order strain derivatives of the dielectric constant tensor. From equ (2.1) it is apparent that the electrostrictive constants depend on the third order coupling parameters among the atoms and the electronic degrees of freedom and therefore represent first order anharmonic effects. Therefore lattice theoretical models of electrostriction must include anharmonic effects to first order in a consistent manner.

2.3.3.2 Shell Models in Lattice Dynamics

The shell model was introduced almost two decades ago (Cochran, 1959; Woods et al, 1960; Cochran, 1961; Dick and Overhauser, 1958; Hardy, 1962) and is now the most widely used theoretical model in the lattice theory of ionic and covalent crystals (See, for example, the review articles by Cochran, 1971, Bilz et al., 1974, and Hardy, 1974). The reasons for its success are that it provides a simple, but sufficiently adequate method for treating effects associated with the electronic polarizability of the ions, and that it explicitly takes into account the difference in the location of the electron shells, which determine the interatomic short-range exchange and overlap forces, and the location of the nuclei, which are associated with the inertial forces. This is achieved by approximating the electronic charge distribution by (rigid) spherical shells which are coupled by means of springs to the ion cores composed of the nuclei and the inner electron shells.

In the rigid ion model (Kellermann, 1940) the interatomic forces are completely specified by the ionic charges $Z_\alpha e$ (e = electronic charge; $\alpha$ labels the different types of ions), which give rise to the long-range Coulomb forces, and the derivatives of the short-range interaction potential $\phi(R)$. The latter are conveniently described by the dimensionless parameters:

$$B_i = \left(\frac{2V}{e^2 R_i}\right)\left(\frac{\partial\phi}{\partial R}\right)_{R=R_i} \tag{2.5a}$$

$$A_i = \left(\frac{2V}{e^2}\right)\left(\frac{\partial^2\phi}{\partial R^2}\right)_{R=R_i} \tag{2.5b}$$

$$C_i = \left(\frac{2VR_i}{e^2}\right)\left(\frac{\partial^3\phi}{\partial R^3}\right)_{R=R_i} \tag{2.5c}$$

$R_i$ (i= 1,2,...) denotes the interatomic distances between first, second, etc. neighbors, and V the volume per unit cell. Alternatively, for the Born-Mayer form of the interatomic potential,

$$\phi(R) = be^{-R/\rho} \tag{2.6}$$

the two parameters b and $\rho$ are required. One of the parameters in (2.6), or one of the parameters $B_i$ according to equ (2.5a) may be eliminated by means of the equilibrium condition. Noncentral forces may be described if the two parameters $A_i$ and $B_i$ are taken as independent, so that they describe the second derivatives of the interatomic potential for displacements parallel and perpendicular to the direction connecting two ions according to

$$A = \left(\frac{2V}{e^2}\right)\left(\frac{\partial^2\phi}{\partial R^2}\right)_{||} \tag{2.7a}$$

$$B = \left(\frac{2V}{e^2}\right)\left(\frac{\partial^2\phi}{\partial R^2}\right)_{\perp} \tag{2.7b}$$

In the original and simplest version of the shell model, the rigid shell model, two additional parameters are required for each polarizable ion. They are the shell charges $Y_\alpha$ and the core-shell force constants $k_\alpha$ which enter the expressions for the electronic polarizability. In later versions of the shell model additional electronic degrees of freedom are introduced, or non-

linear effects are included. For example, in the breathing shell model (Schröder, 1966; Nüsslein and Schröder, 1967) a radial deformation of the electron shell is allowed. In the charge transfer model (Verma and Singh, 1969; Verma and Agarwal, 1973; Feldkamp, 1972) charge transfer between ions is introduced, which gives rise to three-body forces. In the deformable ion model (Jaswal and Dilly, 1977; Jaswal, 1978) the deformation polarizability and the electrical polarizability are taken as different. Among the major achievements of these more elaborate shell models are that they provide better agreement between calculated and measured phonon dispersion curves along different crystallographic symmetry directions with fewer empirical parameters than the rigid shell model, because the short-range interactions need to be considered only up to fewer neighbors. For example, for MgO the charge transfer model gives excellent agreement with six parameters (Verma and Agarwal, 1973), and for ZnS (zinc-blende) only five parameters are required (Jaswal, 1978).

In the charge transfer model (Verma and Singh, 1969; Verma and Agarwal, 1973; Feldkamp, 1972) charge transfer between nearest neighbor ions is introduced as a function of the interionic distance and is described by a function f(R). The additional parameters required in the theory are $f = f(R_o)$; $f' = (df/dR)_{R_o}$ and $f'' = (d^2f/dR^2)_{R_o}$.

All the parameters of the shell model discussed above are required for the description of properties in the harmonic approximation, with the exception of $C_i$ as defined in equ (2.5c) and the charge transfer parameter f" mentioned in the previous paragraph, which are required for the description of first order anharmonic effects, such as the electrostrictive constants. The constants $C_i$ may be either treated as independent empirical parameters, or calculated from the parameters $A_i$, $B_i$ by assuming the Born-Mayer form (2.6) for the interatomic potential.

2.3.3.3 Previous Theories of Electrostriction

In Table 2.2 the theoretical models are specified which have previously been used to account for the electrostrictive constants of alkali halides.

In the rigid ion model of Grindlay and Wong (1969), denoted by RI-1, short-range interaction is considered between nearest neighbors only, and the Born-Mayer potential (2.6) is assumed. The only free parameter of this model is the hardness parameter $\rho$ which is fitted to the static dielectric constant $\varepsilon_o$. For comparison a second rigid ion model, denoted by RI-2, is included in Table 2.1 in which the first neighbor interaction is to be of noncentral type up to second order in the ionic displacements, in which second neighbor interactions of central force type are included, and in which the form of the interatomic potential is not specified. The three harmonic parameters $A_1$, $B_1$, $A_2$ are fitted to the three elastic constants, and the two anharmonic parameters are fitted to the first pressure derivatives of two of the elastic constants.

The shell model (SM) included in Table 2.2 is a generalized version of the model considered by Srinivasan and Srinivasan (1972). It differs from RI-2 in that the polarizability of the anions, described in terms of the two additional parameters Y and k, is included, and in that the five harmonic parameters are determined from the three elastic constants, from the static and optical dielectric constants $\varepsilon_o$ and $\varepsilon_\infty$ respectively, and from the transverse optical frequency $\omega_{TO}$.

In the model of Goyal et al. (1978), denoted by SM-MB, three-body forces arising from the charge transfer mechanism are included, but short-range forces are considered only between first nearest neighbors, are assumed to be of central force type, and are described by a Born-Mayer potential. Therefore, the only anharmonic parameter is the second derivative f", which is fitted to the pressure coefficient of the bulk modulus.

Table 2.2 Previous theoretical models used for calculation of electrostrive constants.

| Model | Authors | Interactions | Parameters | | Exp. Input | |
|---|---|---|---|---|---|---|
| | | | Harmonic | Anharmonic | Harmonic | Anharmonic |
| RI-1 | Grindlay and Wong (1969) | Coulomb<br>1.n.n. central | $\rho$ | | $\varepsilon_o$ | |
| RI-2 | | Coulomb<br>1.n.n.general<br>2.n.n.central | $A_1$, $B_1$<br>$A_2$ | $C_1$<br>$C_2$ | $c_{11}, c_{12}, c_{44}$ | $\frac{\partial c_{11}}{\partial p}$, $\frac{\partial c_{44}}{\partial p}$ |
| SM | Srinivasan and Srinivasan (1972) | Coulomb<br>1.n.n.general<br>2.n.n.central<br>polarizable anions | $A_1$, $B_1$<br>$A_2$<br>Y,k | $C_1$<br>$C_2$ | $c_{11}, c_{12}, c_{44}$<br>$\varepsilon_o, \varepsilon_\infty, \omega_{To}$ | $\frac{\partial c_{11}}{\partial p}$, $\frac{\partial c_{44}}{\partial p}$ |
| SM-MB | Goyal, et al. (1978) | Coulomb<br>1.n.n.central<br>polarizable anions<br>long-range three body | $\rho$<br>Y,k<br>f,f' | f" | $c_{11}, c_{12}, c_{44}$<br>$\varepsilon_o, \varepsilon_\infty, \omega_{To}$ | $\frac{\partial B}{\partial p}$ |

RI = Rigid ion model; SM = shell model; MB = many body force model.

In Table 2.3 the experimental electrostrictive constants in Voigt notation* and the pressure coefficient of the static dielectric constant** are compared with the results calculated from the four models for two selected alkali halides. In order to eliminate variations arising from different input parameters the values recalculated by us from identical input parameters are given instead of the values calculated by the original authors. The experimental values are from Bohatý and Haussühl (1978).

It is apparent that for NaCl model SM-MB gives the best overall agreement and the correct sign for $f_{44}$. However, for $f_{12}$ model RI-2 gives the best agreement, and the value of $f_{44}$ for model SM-MB is far too small. For KBr model RI-1 gives the best overall agreement. However, only models SM and SM-MB give the correct sign of $f_{44}$, although again the calculated coefficients are far too small. For NaCl model RI-2 gives the best agreement for $f_{12}$, and for KBr both models RI-1 and RI-2 give the best, but still very poor agreement for $f_{12}$.

The relatively good agreement (which is, though, still far from satisfactory) obtained for KBr with the rigid ion model RI-1 is surprising and must be attributed to a cancellation of errors, because the model is the simplest of all models considered and does not include electronic polarizability. Therefore the optical dielectric constant would be equal to one, and all piezooptic constants would be zero.

---

*Index pairs (ij) occurring in tensor notation are replaced by single indices $\mu$ according to the scheme (ij) = 11,22,33,23 and 32,13 and 31, 12 and 21 → $\mu$ = 1,2,3,4,5,6.

**This quantity is related to the electrostrictive constants defined by (2.1) and (2.3) according to

$$\left(\frac{\partial \epsilon_o}{\partial p}\right) = \left(\frac{2}{3B}\right)(f_{11} + 2f_{12})$$

where B denotes the bulk modulus.

Table 2.3 Comparison of experimental and calculated electrostrictive constants (in $10^{-10}$ N/V$^2$) and pressure coefficients of the static dielectric constant $\varepsilon_o$ (in $10^{-10}$ N$^{-1}$ m$^2$) for NaCl and KBr.

| | Model | $f_{11}$ | $f_{12}$ | $f_{44}$ | $\frac{1}{\varepsilon_o}\left(\frac{d\varepsilon_o}{dp}\right)$ |
|---|---|---|---|---|---|
| NaCl | Experiment | -2.67 | 0.62 | -0.97 | -1.04 |
| | RI-1 | -3.03 | 0.36 | 0.17 | -1.19 |
| | RI-2 | -5.03 | 0.55 | 0.35 | -2.04 |
| | SM | -2.23 | 0.21 | 0.009 | -0.95 |
| | SM-MB | -2.56 | 0.19 | -0.03 | -1.26 |
| KBr | Experiment | -2.56 | 0.82 | -0.66 | -1.25 |
| | RI-1 | -2.57 | 0.31 | 0.15 | -2.06 |
| | RI-2 | -5.32 | 0.31 | 0.15 | -4.97 |
| | SM | -1.98 | 0.08 | -0.09 | -1.94 |
| | SM-MB | -2.47 | 0.11 | -0.08 | -2.57 |

Model SM-MB is the most elaborate and realistic of the models considered in that electronic polarizability effects are included and even some form of anharmonicity of the electron shells is taken into account through the charge transfer parameter f". However, as will be discussed in Section 2.3.3.4, the anharmonic shell effects are treated in an inconsistent manner in SM-MB. In addition, other potentially important effects are omitted in SM-MB, such as nonlinearity of the core-shell coupling, and second neighbor short-range repulsive forces. Perhaps the relatively poor agreement of this model for KBr could also be attributed in part to the neglect of cation polarizability.

Clearly, theoretical work on electrostriction in piezoelectric and ferroelectric crystals can only be started after an adequate model and an adequate theory for electrostriction in alkali halides are available. The objective of the work pursued under the present contract is to develop such a theory and to provide this theoretical framework for subsequent application to piezoelectric and ferroelectric materials.

2.3.3.4 Lattice Dynamics of Anharmonic Shell Models

The lattice dynamical framework for the calculation of numerous anharmonic properties has been derived and/or reviewed by Cowley (1964,1965). However, as first pointed out by Oitmaa (1967) the anharmonicity included by Cowley and most of the subsequent applications refers only to the nonlinearity of the interionic forces with respect to ionic displacements, but the anharmonicity associated with the intraionic forces is neglected, that is the core-shell coupling is harmonic. Notable exceptions are calculations of thermal expansion based on the quasiharmonic approximation (See for example the review article by Glyde and Klein, 1971), of the second-order Raman spectra of alkali-earth oxides (Rieder et al., 1973; Migoni et al., 1976), and of the mode

softening in $KTaO_3$ (Migoni et al., 1978). The thermal expansion calculations are based on a volume dependent core-shell force constant, and in the theory of the second order Raman spectra and of the mode softening a quartic term in the displacements is introduced in the energy for the core-shell displacements and is found to be of crucial importance.

Since the electrostrictive coefficients describe the strain dependence of the static dielectric constant tensor, and since the dielectric constant includes electronic polarizability effects it would appear mandatory to include intraionic anharmonicity in any adequate theory of electrostriction. As mentioned in Section 2.3.3.2 the only model in which this is attempted, SM-MB, it is done, however, in a manner which is inadequate for the following three reaons: First, the primary feature of intraionic anharmonicity, the nonlinear core-shell coupling is not taken into account. Second, the anharmonicity resulting from the charge transfer mechanism primarily affects the interionic forces, but not the intraionic forces. Third, the anharmonic effects are introduced in the equations derived by Srinivasan (1968), which refer to a shell model with purely harmonic intraionic forces. As pointed out by Oitmaa (1967), the effective anharmonic coupling parameters for a fully anharmonic shell model depend in an essential manner on the intraionic anharmonicity.

In the present work the effective coupling parameters have been derived consistently for a fully anharmonic shell model, including both interionic and intraionic anharmonicity. With these correct expressions exact and general expressions for the pertinent first order anharmonic coefficients are being derived at present. This includes the third order elastic constants, the photoelastic coefficients, and the electrostrictive coefficients. Application to simple crystal structures, especially the rocksalt, zincblende and perovskite structures, is planned for the future.

### 2.3.4 Summary and Conclusions

All previous theoretical treatments of the electrostrictive constants are inadequate from a theoretical point of view and because of poor agreement with the experimental data for alkali halides. We are in the process of deriving consistent and general equations for the first order anharmonic material constants, including the electrostrictive constants, in which anharmonic effects associated both with interionic and intraionic forces are included. Considerable improvement of the agreement between theory and experiment is expected for alkali halides, and subsequent application to piezoelectric and ferroelectric materials is planned.

## 2.4 References


Bilz, H., Gliss, B. and Hanke, W. (1974) in Dynamical Properties of Solids, Vol. 1 (edited by G.K. Horton and A.A. Maradudin) p. 343 (North Holland, Amsterdam).

Bohatý, L. and Haussühl, S. (1977) Acta Cryst A33, 114.

Cochran, W. (1959) Proc. Roy. Soc. Lond. A253, 260.

Cochran, W. (1961) Adv. Phys. 9, 387.

Cochran, W. (1971) Crit. Rev. Sol. State Sci. 2, 1.

Cowley, R.A. (1963) Adv. Phys. 12, 421.

Cowley, R.A. (1965) Phil. Mag. 11, 673.

Dick, B.G. and Overhauser (1958) Phys. Rev. 112, 90.

Feldkamp, L.A. (1972) J. Phys. Chem. Sol. 33, 711.

Glyde, H.R. and Klein, M.L. (1971) Crit. Rev. Solid State Sci. 2, 181.

Goyal, S.C., Prakash, R. and Tripathi, S.P. (1978) Phys. Stat. Sol.(b)85, 477.

Grindlay, J. and Wong, H.C. (1969) Can. J. Phys. 47, 1563.

Hardy, J.R. (1962) Phil. Mag. 7, 315.

Hardy, J.R. (1974) in Dynamical Properties of Solids, Vol. 1 (edited by G.K. Horton and A.A. Maradudin) p. 157 (North Holland, Amsterdam).

Jaswal, S.S. (1978) J. Phys. C: Solid State Phys. 11, 3559.

Jaswal, S.S. and Dilly, V.D. (1977) Phys. Rev. B15, 2366.

Kellermann, E.W. (1940) Phil. Trans. Roy. Soc. A238, 513.

Kinase, W. and Itoh, M. (1977) J. Phys. Soc. Japan 42, 895.

Migoni, R., Bilz, H. and Bäuerle, D. (1976) Phys. Rev. Lett. 37, 1155.

Migoni, R., Bilz, H. and Bäuerle, D. (1978) in Lattice Dynamics (edited by M. Balkanski), p. 650 (Flammarion, Paris).

Nüsslein, V. and Schröder, U. (1967) Phys. Stat. Sol. 21, 309.

Oitmaa, J. (1967) Australian J. Phys. 20, 495.

Rieder, K.H., Weinstein, B.A., Cardona, M. and Bilz, H. (1973) Phys. Rev. B8, 4780.

Schröder, U. (1966) Solid State Commun. 4, 347.

Srinivasan, R. (1968) Phys. Rev. 165, 1041.

Srinivasan, R. and Srinivasan, K. (1972) J. Phys. Chem. Sol. 33, 1079.

Verma, M.P. and Singh, R.K. (1969) Phys. Stat. Sol. 33, 769.

Verma, M.P. and Agarwal, S.K. (1973) Phys. Rev. B8, 4880.

Woods, A.D.B., Cochran, W. and Brockhouse, B.N. (1960) Phys. Rev. 119, 980.

# 3. PIEZOELECTRIC COMPOSITES

## 3.1 Introduction

Earlier studies on ONR contract N00014-76-C-0515 have demonstrated quite clearly that for voltage generating devices such as hydrophones, where the figure of merit for the piezoelectric material involves the hydrostatic voltage coefficient $g_h$, or a produce $g_h d_h$, composite piezoelectrics can be fabricated which have properties which are superior to those of either single component.

In the earlier study, a ceramic:plastic composite of controlled phase interconnection[3.1] was fabricated by a ceramic replication process, using the three dimensionally porous coral porites:porites as a template structure[3.2]. The reasons for seeking to control the phase interconnection in diphasic systems which try to exploit coupled properties, as in the electromechanical transducer, have been given in detail in 3.1. The replication process by which coral was exploited as a template microstructure to produce the required form of phase interconnection for a transducer with high hydrostatic sensitivity has been given in 3.2.

A significant disadvantage of the replamine process described in 3.2 as a mode for reproducing a 3:1 connected structure, is that it is topologically impossible to use the template more than once, i.e. a new block of the template material of suitable size and shape is required in the fabrication of each device. Both theoretical studies in this Laboratory[3.3] and recent macro-modeling studies at NRL[3.4] have confirmed, however, that the ideal phase connection for the type of transduction required is really 3:1 and not full 3:3.

In the replamine studies this was also apparent, as the coral porites: goniopera which has a preferred anisotropy in its structure with strong connections in 1 dimension, and weaker links in the two orthagonal directions gave better results than the more isotropic porites:porites.

Fortunately, 3:1 connection is in many ways more simple to architect in a composite than is the 3:3 structure of the coral. In these new studies, two methods are being explored for the fabrication of ceramic:plastic composites with dominant 3:1 connectivity and a range of scales in the microstructure.

The first is a modification of the original replamineform process, but using now a manufactured prototype structure of fine steel rods on regularly spaced centers. Again a wax negative is made from the master template, but now after the wax has set the template can be extracted and reused many times.

In the second effort, which started over the last three months, very fine PZT rod is being extruded. These PZT fibers appear to offer intriguing possibilities for manipulation in the flexible green state to form a wide range of composites with 3:1 and with other more complex modes of interconnection.

## 3.2 Casting from Metal Template Structures

The basic idea was to generate a structure of regularly spaced columns of PZT supported on a PZT base plate, on a scale where the columns could be down to 100 μmeters in diameter and arranged in a regular two-dimensional pattern. The most obvious template for this type of structure is a wire brush, with bristles of the required diameter arranged on regularly spaced centers. After the wires have been coated with a suitable parting agent, wax can be cast around the wires. When the wax has set, the wires can be withdrawn, leaving a wax template with regularly spaced columnar holes. The holes can now be filled with a PZT slip by vacuum impregnation, the slip dried, the wax melted out and the ceramic fired, just as in the replamine process.

The major advantage would be that the template is not destroyed, but is removed intact, so that an expensive carefully prepared template could be reused many times in the process. Since the scale of wire used, and the spacing,

are open to choice, intentionally periodic structures could be fabricated with the scale and the periodicity controllable in the plane of the template.

The flow sheet for the processing, which is closely similar to that of the replamine processing is given in Fig. 3.1.

Initial experiments were carried out using a low-density structure consisting of 8 steel rods 300 μmeters in diameter 1 cm long, spaced around the perimeter of a 5 mm diameter circle. The casting wax used was a Kerr inlay wax, though subsequent experiments have used a number of different natural and synthetic waxes. Investment of the wax megatives was with a PZT 501 slip, and the integrity of the invested PZT columns was checked by x-ray shadow photography.

A major problem with this method occurs at the stage of wax removal. The meltdown operation is exceedingly critical, the melting wax breaking up the fragile PZT columns. Once the wax is removed there appeared to be no serious problem in firing the PZT columns without serious warpage.

Experiments are now proceeding along the following lines:

1. Improving the drying of the PZT slip by using vacuum drying and microwave heating.

2. Strengthening the PZT columns by decreasing the height and thus increasing the diameter-to-height ratio.

3. Experimenting with "abrupt" melting synthetic waxes which may be melted by radiant heat from the surface, i.e. melting back layer by layer.

4. Testing campher based waxes which sublime directly without melting.

5. Using a thin layer of slip on both surfaces of the wax replica (using a much higher density of rods) so that the rods are supported at both ends as the wax melts out.

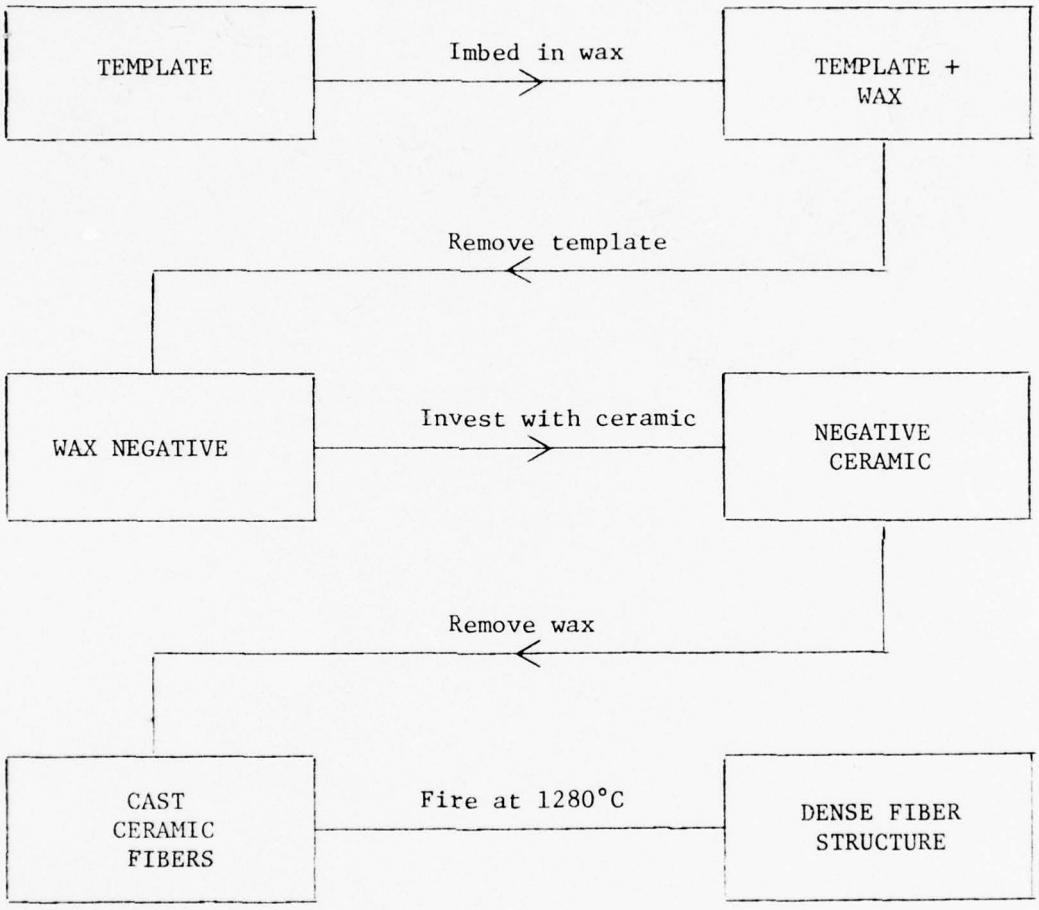


Fig. 3.1 Flow chart for lost wax casting process of replication.

Our experience to date suggests that the template structures can be generated and controlled quite easily, and offer a very wide range of possibility both in scale factor and in make-up in the plane. If the step of wax removal can be accomplished satisfactorily, the method should make an interesting and more controllable alternative to the present replamine processing.

### 3.3 Extrusion of PZT Fibers

An attractive alternative to the processing discussed above would clearly become possible if the PZT itself could be fabricated as a fine fiber. Preliminary studies with a rather simple extrusion press suggest that this may in fact be possible for an extensive range of fiber diameters.

The extrusion apparatus which has been used consists of a small Carver Model M hydraulic laboratory press, a one-inch diameter ram and die set with a detachable end plate. The paste is extruded through a single hole in the end plate, and to avoid curling of the extruded fiber it was found desirable to use an extrusion channel which is as long as possible. For the present experiments holes of 40, 30, 20 and 13 thousandths of an inch (mils) have been used. The 40 and 30 mil holes were drilled in 3/4" plate, the 20 and 13 mil extrusion holes in 5/8" plate.

The paste used for these studies was of a commercial PZT 501A formulation and was made up from 90 wt% PZT, 8 wt% water, and 2 wt% polyvinyl alcohol (PVA). The paste was ball milled in a plastic lined mill for 12 hours then extruded several times through a 40 mil die to ensure homogeneity.

After the extruded fiber has dried in air, it is cut into suitable lengths, and the binder burned out over a 1/2 hour period at 550°C. Sintering was carried out at 1310°C in a closed crucible with control of the PbO partial pressure. For the single fibers, densities greater than 95% of theoretical

have been obtained. Both straight and curved fibers have been fired, and it appears that the general shape imparted in the green state can be preserved through the firing process.

Work is now in progress exploring various methods for processing and assembling fiber based composites.

## 3.4 References


3.1 R.E. Newnham, D.P. Skinner and L.E. Cross. Mat. Res. Bull. 13, 525 (1978).

3.2 D.P. Skinner, R.E. Newnham and L.E. Cross. Mat. Res. Bull. 13, 599 (1978).

3.3 L.E. Cross. Bull. Am. Ceram. Soc. 57, 768 (1978).

3.4 R. Pohanka, R. Rice and P. Smith. NRL Memorandum Report 3854. Advanced Ceramics and Composites for Underwater Acoustic and Engineering Applications, October 1978.

# 4. GRAIN ORIENTED CERAMICS

## 4.1 Introduction

Mixed bismuth oxide compounds with layer type structures form an extensive family of ferroelectrics with large spontaneous polarizations and high Curie temperatures. The prototypic symmetry for the family is 4/mmm, and most members have ferroelectric phases in orthorhombic mm2 with only four equivalent planar orientations for $P_s$. While the Curie temperatures, polarizations, and electrostriction constants suggest that the family should be of major interest for piezoceramic applications, the large planar anisotropy prevents effective poling of a randomly axed polycrystal.

Some few years ago we proposed to investigate, in an earlier ONR program, the possibility of generating grain oriented ceramics with a dominant planar anisotropy, so that the poling field could be always in a plane of easy ferroelectric switching and the ceramic could be poled. Unfortunately the resources were not adequate to undertake this topic.

In the meantime, recent studies in Japan[4.1,4.2,4.3] have produced excellent grain oriented $Bi_4Ti_3O_{12}$, and other compositions in the layer structure family using a uniaxial hot-pressing technique which permits limited extrusion. This clever process produces most effective orientation in the ceramic grain structure for samples fabricated from powders which exhibit little or no shape anisotropy. It is, however, an expensive process for manufacture.

In the present program we are exploring an alternative approach which may be significantly less expensive and appears accessible for a wide range of the layer structure compounds.

## 4.2 Fused Salt Processing of Layer Structure Oxides

Our approach is to use a synthesis step which appears to permit the

fabrication of powders in the bismuth oxide layer structure family which have a marked platey morphology. These powders can then be processed by a range of conventional ceramic forming techniques, sedimentation, tape casting, slip casting, etc. which are known to preserve the built-in anisotropy of the powder.

It is an observation of almost all attempts to grow single crystals of the bismuth titanate $Bi_4Ti_3O_{12}$ that whatever the flux system, the crystals grow with a mica-like habit and extremely platey morphology. Thus we were tempted to try rapid exsolution from a molten salt bath as a possible technique for generating microcrystals.

The flux used was a 1:1 mixture of KCl:NaCl. For $Bi_4Ti_3O_{12}$ stoichiometric proportions of the $Bi_2O_3$ and $TiO_2$ were mixed with the 1:1 salt in weight ratios 1:1 up to 1:10. After milling the mixtures were fired in a covered alumina or platinum crucible to a temperature of 1150°C, then cooled at the free running furnace cooling rate. After cooling, the salt was dissolved out by repeated washing in water and the powders were dried.

A typical scanning electron micrograph of the powder produced in this manner is shown in Fig. 4.1, where the very plate-like character is obvious. Contrary to our initial expectation, the average particle size in the major dimension did not depend markedly upon the cooling rate of the flux. Slow cooling appeared to give rather more angular particles with better developed (hkO) faces, but neither the major dimensions of the sheets nor the thickness was markedly increased by the slower cooling rates.

A similar family of experiments have been carried through for the compound bismuth tungstate ($Bi_2WO_6$). In this system a slightly lower maximum firing temperature appeared to produce optimum results. A scanning electron micrograph of this powder is shown in Fig. 4.2.


Fig. 4.1 $Bi_4Ti_3O_{12}$ powder produced by molten salt process. Scanning electron microscope picture magnification indicated.


Fig. 4.2 $Bi_2WO_6$ powder produced by molten salt process. Electron micrograph magnification indicated.

Experiments are now proceeding to tape cast grain oriented ceramic sheets from these precursor powders. The initial results with $Bi_4Ti_3O_{12}$ look most encouraging with x-ray diffraction showing a strongly preferred c orientation normal to the plane of the fired sheets.

## 4.3 References


4.1 K. Okazaki. Report on the Workshop on Sonar Transducer Materials, U.S. NRL, Washington DC, Nov. 13-14 (1975).

4.2 H. Igorashi, K. Matsunaga, T. Taniai and K. Okazaki. J. Am. Ceram. Soc. 57, 815 (1978).

4.3 H. Igorashi, T. Taniai, M. Itiguchi and K. Okazaki. Bull. Am. Ceram. Soc. 57, 768 (1978).

# 5. FERROELECTRIC CRYSTAL GROWTH

## 5.1 Introduction

The rationale for establishing crystal growing capability on this program has been discussed earlier. Since the solid solution materials which are of most interest are all necessarily incongruently melting, flux growth techniques are required, and the initial focus has been in this area. The Laboratory has had a long history of successful high temperature flux growth with other oxide systems, but recently this activity has been reduced, so much of the work accomplished over the first months of this contract has of necessity been concerned with refurbishing and updating the furnaces and temperature control equipment for these new studies.

In the following a brief description is given of the vertical de-mountable type furnace which is being used so as to permit the flux to be decanted before solidification, and of the new high precision μ data-track system which has been installed to permit the precise program control of two furnaces. The use of this equipment to grow single crystals of lead magnesium niobate for electrostriction studies is described, and the present ongoing program for growing $Pb_3MgNb_2O_9$:$PbTiO_3$ and $PbZrO_3$:$PbTiO_3$ crystals briefly reviewed.

## 5.2 Furnace and Control Equipment

The demountable tube furnace is of rather simple construction. The mullite inner sheath, closed at one end, is approximately 21" long and 5" in diameter. This tube is supported on a firebrick base surrounding a 3-3/4" diameter lower entry hole, and is inside a rectangular box formed by high temperature insulating bricks held in a Syndanyo sheet chamber. The top of the chamber is composed of removable bricks drilled to accommodate four Crystolon spiral-cut silicon carbide heating elements.

The crucible to be heated is supported on a fixed alumina column which enters through the lower entry hole. The whole furnace box is mounted on vertical rails and is counterweighted so that it lifts off the alumina pedestal allowing easy access to the growth crucible.

The temperature controlling thermocouple is attached to the sheath tube at the hot zone, and moves with the furnace. The temperature sensing couple is at the top of the support pedestal in contact with the growth crucible.

Power level required to maintain the furnace at 1300°C is about 6KVA (30 amps at 200 volts).

A stop on the demount rails positions the crucible in the hot zone of the furnace, but final positioning can be trimmed by a lab jack under the pedestal structure.

Temperature control for the furnace is provided by a Research, Inc. 640 U temperature control unit regulating the output of a Payne 80 amp phaser unit. The control program is established by a new Research, Inc. μ data-track digital controller with Master and Blend station set. These units, together with a Fluke digital thermometer, voltmeter and ammeter for the furnace current and the appropriate switches, are mounted in a mobile rack unit (Fig. 5.1).

The heart of the control system is the μ data-track unit. Working on a 12-bit digital coding, the unit provides a control voltage resolution of 1/4000. Using a Master and Blend station unit, however, this control signal can be arranged to cover anything from 0 - 100% of the full temperature range, i.e. shorter segments of the temperature range can be covered with very high resolution as is often required in crystal growth.

In the simplest form, the microprocessor based controller which is timed by its own internal clock breaks the program into 19 linear segments, duration and rate of change in each segment being controllable over a very wide range. With pre-programmed ROM the resolution can be further improved to 127 linear

program segments, each with duration 1 to 1,999 seconds, minutes, or hours. Transfer between program segments can also be used to activate relay closure, and up to seven external commands can be generated by the system for ancillary functions.

In conjunction with the demountable box kiln, the controller provides a very precise but highly flexible system. With the Master and Blend stations two completely independent control program signals can be generated, and we anticipate adding a second furnace to complete the unit.

## 5.3 Growth of Lead Magnesium Niobate

Lead magnesium niobate $Pb(Mg_{1/3}Nb_{2/3})O_3$ crystals were grown from a flux of excess PbO with $B_2O_3$, using a composition ratio which had been found to work by Banner and Van Uitert[5.1] for crystal pulling by the Kyropoulos technique.

The mole fractions of the starting oxides were PbO:0.6M, MgO:0.2M, $Nb_2O_5$: 0.06M, $B_2O_3$:0.14M. Care must be taken in precalcining the MgO powder to avoid hydration. The oxides were wet mixed, then melted down into a platinum crucible.

The temperature program involved a preheat to 400°C, held at that temperature for several hours to fully oxidize the lead and reduce the likelihood of reduced PbO reacting with the crucible, rapid heating to 1150°C followed by a soak of 2 hours at temperature. The melt was cooled at 3°/hour to 950°C, at 10°/hour to 850°C, followed by rapid cooling to room temperature.

The flux was not poured off in these initial runs, and the crystals were extracted from the matrix by boiling in 20% nitric acid solution.

The crystals grown were light yellow in color with nearly perfect <100> cube faces and edge lengths in the range 1-2 mm (Fig. 5.1). Transmitted light microscopy shows most of the crystals to be free from major flux inclusions, isotropic in polarized light and free from any evidence of a gross twin structure.

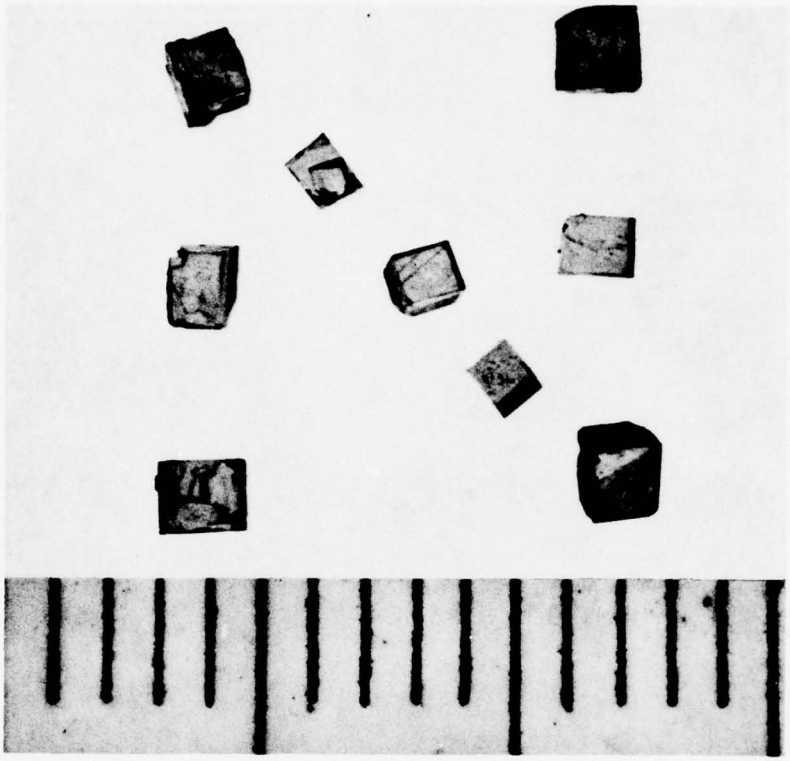

Fig. 5.1 Flux grown crystals of $PbMg_{1/3}Nb_{2/3}O_3$. Scale marks are millimeters.

In the thicker samples, the edge regions exhibit parallel extinction, but this is probably due to total internal reflection at the inside surfaces. The body of the crystals appears strain and extinction free.

Preliminary dielectric measurements show a high dielectric maximum at temperature just below room temperature which appears dispersive as is expected in the lead magnesium niobate.

## 5.4 Growth of PZT Solid Solution Crystals

It should be stressed at the outset that the goal of this longer range program is not to produce large crystals of PZT for any practical application. The requirement is for very small homogeneous crystals with simple twin structures which can be de-twinned mechanically and electrically, so that the single domain properties are accessible for study. Thus the critical features are homogeneity in the cation distribution, perfection and morphology. Size is of very minor importance.

Writing the formula for the PZT family in the form $Pb2r_xTi_{(1-x)}O_3$, the values of x covering the range 0.10 to 0.80 are of most importance, since this covers the full range of simple proper ferroelectric compositions and encompasses the important region of morphotropy.

In the initial phase of the present approach, four avenues are presently being explored. For PZT feed stock, both simple mixed oxides and precalcined "homogenized" PZTs are being tried. Two flux systems are also being employed. The first comprises a mixture of lead fluoride potassium fluoride and lead phosphate, which has been used successfully by Rosolowski and Arendt for the growth of x = 0.50 PZTs. The second was suggested by recent work at General Electric Company, where highly reproducible PZT powders are being produced from a KCl:NaCl eutectic melt.

To date, only some 10 growth runs have been attempted. In each case a fixed 15:85 weight ratio of PZT:flux was used and heating was carried out in a small 50 cc platinum crucible.

For the fluoride:phosphate flux the temperature cycle involved rapid initial heating (3 to 3-1/2 hours), a 3-hour soak at 1210°C, cooling to 810°C over a period of 1-1/2 to 5 hours, then a rapid cool down to room temperature. In several runs the flux was poured off at 810°C; for one or two, the flux was solidified in the crucible.

In each case, small single crystals were obtained. A typical example is shown in Fig. 5.2 from a run with x = 0.80. Here the optical properties show clear straight extinction in polarized light, indicating that the grown composition is in the rhombohedral phase field at room temperature. High temperature microscopy is now underway with these crystals to determine the homogeneity of the Curie temperature within a single crystal, and between crystals of the same batch.

Further effort is obviously required to modify the growth process to improve the perfection.

For the KCl:NaCl flux, less work has been carried out, and the initial results do not look encouraging. Soak tests carried out on the mixed oxide compositions at 950°C suggest that while the PbO is rapidly digested in the flux, $ZrO_2$ and $TiO_2$ remain. We propose now to experiment with organically prepared PZTs as the starting material to see if this will dissolve in the flux. If these experiments are not successful, all effort will be concentrated on the other flux system.

## 5.5 Reference

5.1 W.A. Bonner, L.G. Van Uitert. Mat. Res. Bull. 2, 131 (1967).

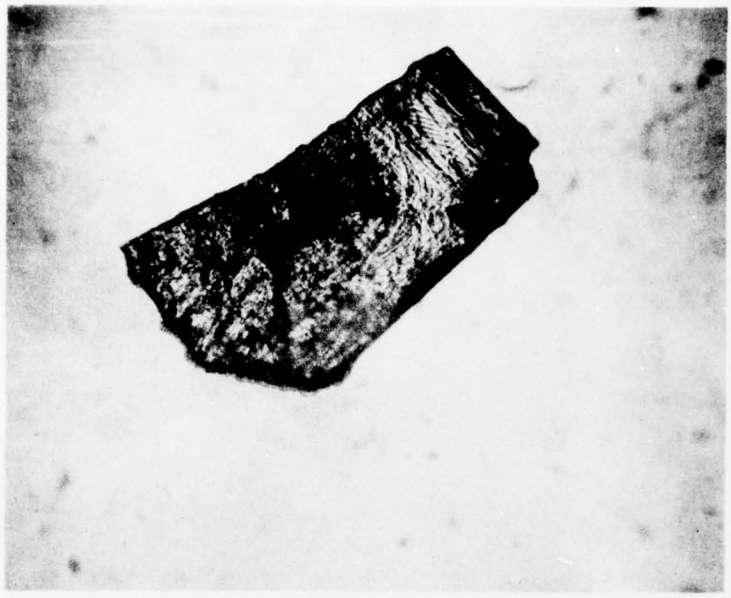

a)

b)

Figure 5.2 Rhombohedral crystal from Run 801-692-102 shown in a) transmitted unpolarised light and b) transmitted polarised light to illustrate the development of domains.

# 6. STUDIES OF FERROELECTRIC BICRYSTALS

## 6.1 Introduction

The initial objective of these studies is to produce "joining" between differently oriented ferroelectric crystals, along an extended planar boundary, which will simulate as far as possible the character of a single grain boundary in a ferroelectric ceramic. Such planar macro boundaries would permit the measurement of dielectric, optical and elastic properties and a possibility for untangling the complex interaction of elastic and electric boundary conditions on the single crystal properties, and on the evolution of the domain structures in the ferroelectric phases.

In normal ferroelectric ceramics the grain boundaries do encompass quite a range of perfection, of width, and of chemical character from the near perfect co-joining of the narrow angle grain boundary to the very broad second phase inclusion in some deliberately diphasic systems. It is thus of interest to look at a range of techniques and of ferroelectric systems before making detailed choices for specific study.

## 6.2 Experimental Approach

Two possible techniques for producing planar grain boundaries have already been proposed[6.1] viz: direct Czochralski growth of two oriented seed crystals in a suitable melt until the crystals impinge, or alternatively diffusion bonding between two oriented single crystals under pressure at high temperature. The two methods are compared in Table 6.1. In view of the comparative simplicity of the diffusion bonding technique, this approach has been attempted first.

It has been reported[6.2] that in the presence of a suitable solvent many powdered materials can be pressed to high density at temperatures at or below room temperature. Examples include the ice/methanol and sodium chloride/water systems. The solvent acts as a high diffusivity medium for material transfer

Table 6.1 Comparison of Bicrystal Preparation Methods

| Method | Conditions | Product |
|---|---|---|
| 1. Czochralski | Requires accurately oriented, flaw-free seed crystals, a suitable melt, and development of the correct growth techniques for each composition required. | Grain boundary free from secondary boundaries introduced by recrystallization. Possible contamination from the melt if a flux is used. No direct comparison between the properties of the original crystals and the bicrystal is possible. |
| 2. Diffusion bonding | Can be prepared from a single crystal by cutting the crystal and grinding to give the required orientation. Requires a material with sufficient atomic mobility at the bonding temperature. | Grain boundary is directly comparable to those produced in sintering and hot pressing. Second phases can be incorporated in the boundary prior to diffusion bonding. Direct comparison between the properties of the original crystal and the bicrystal can be made. Contamination during grinding and polishing and recrystallization due to strain introduced during grinding may occur. |

during deformation. In many ways the process is analogous to liquid-phase sintering. It should be possible, therefore, to prepare bicrystals from water soluble ferroics such as TGS and KDP. Attempts have been made to produce TGS bicrystals using this method.

### 6.2.1 Diffusion Bonding

Specimens for diffusion bonding are prepared as follows: After measuring its dielectric properties, a single crystal is cut in half using a string saw to minimize structural damage. The halves are then ground and polished on one face in the appropriate orientations until surface irregularities are reduced to the submicron level. Diffusion distances required to remove them entirely and permit bonding are then similar to those encountered in normal sintering and hot pressing.

A simple hot press, shown in Fig. 6.1, has been built to bond the crystals. The specimen is heated using a platinum 40% rhodium wound tube furnace capable of attaining 1500°C. Pressure is applied by deadweight loading through two accurately aligned alumina rods with parallel ground contact faces. Reaction between the alumina rods and the specimen is minimized using platinum foil, which also serves to smooth out stress gradients. Materials subject to composition change by vaporization, such as PZT, are sealed in platinum foil prior to heating. The press has been designed to apply typical hot-pressing pressures (10-50 $MNm^{-2}$) on crystals in the 1-4 $mm^2$ size range. These small crystals are cheap and comparatively easily grown and quite flaw free.

The hot press has been used to prepare a bicrystal of quartz at 1350°C and 10 $MNm^{-2}$ pressure. Bicrystals of $BaTiO_3$, $SrTiO_3$, KTN, PZT and other materials will be made as crystals become available from flux growth work.

### 6.2.2 Solution Bonding

Attempts have been made to form TGS bicrystals at room temperature by

FIGURE 6-1

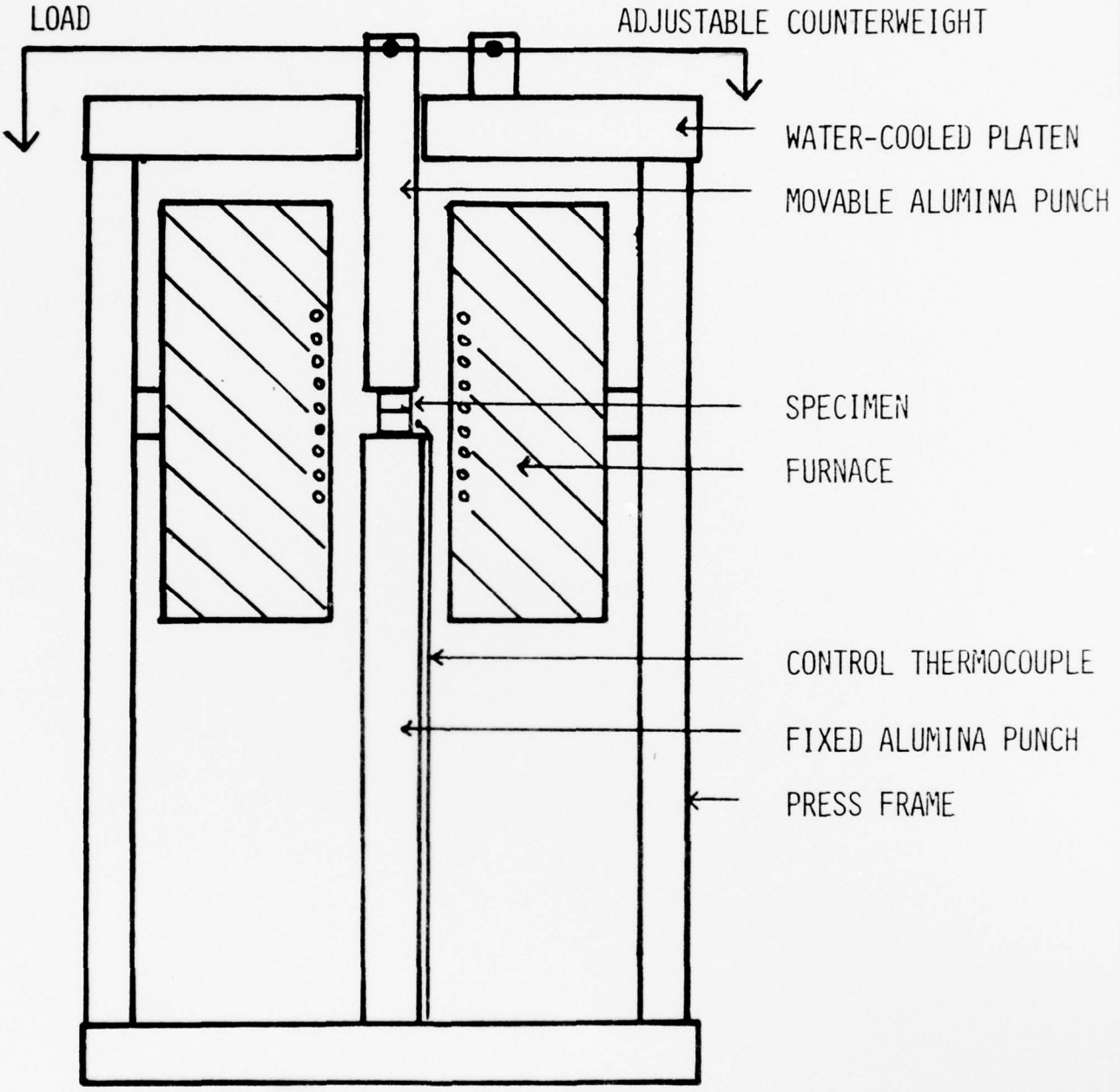
LOAD
ADJUSTABLE COUNTERWEIGHT
WATER-COOLED PLATEN
MOVABLE ALUMINA PUNCH
SPECIMEN
FURNACE
CONTROL THERMOCOUPLE
FIXED ALUMINA PUNCH
PRESS FRAME

pressing together two single crystals with a layer of saturated TGS solution between them. The contact faces of the two crystals were first highly polished using powdered tin oxide and ethanol as a polishing medium. Pressures were kept below 1 $MNm^{-2}$ since higher pressures invariably fractured the crystals. No attempt was made to control the pressing temperature. After allowing two days to reach equilibrium the crystals were desiccated in high vacuum ($10^{-6}$ mm Hg) at 60°C to evaporate any remaining solution.

So far this "diffusion bonding" method has failed to produce a strong bond between the crystals. On examination, evidence of severe etching was found on the contact faces of the separated crystals, but no regions where bonding had apparently taken place. Accordingly, a "crystal growth" approach has been adopted. The crystals were polished as described previously and placed together horizontally with the thickest possible layer of saturated TGS solution between them, but without pressure. After two days at room temperature the crystals were desiccated under vacuum overnight, sectioned, and etched with water and examined by scanning electron microscopy. Figure 6.2 shows that bonding has occurred between the crystals in isolated regions, but many large pores remain. The bonded region is quite thick, as evidenced by preferential etching, and is probably not as crystallographically perfect as the original crystals. This may be associated with surface damage incurred during polishing.

In order to maximize the bonded area between the crystals it is necessary to raise the initial concentration of the TGS solution as much as possible. Unfortunately, a high solution concentration precludes etching of the TGS crystals and prevents the formation of clean contact surfaces. Using the simple model in Fig. 6.3a, it can be shown that for unit area of TGS/solution interface,

$$\Delta L = \frac{L\Delta C}{2\rho}$$

FIGURE 6-2 TGS BICRYSTAL

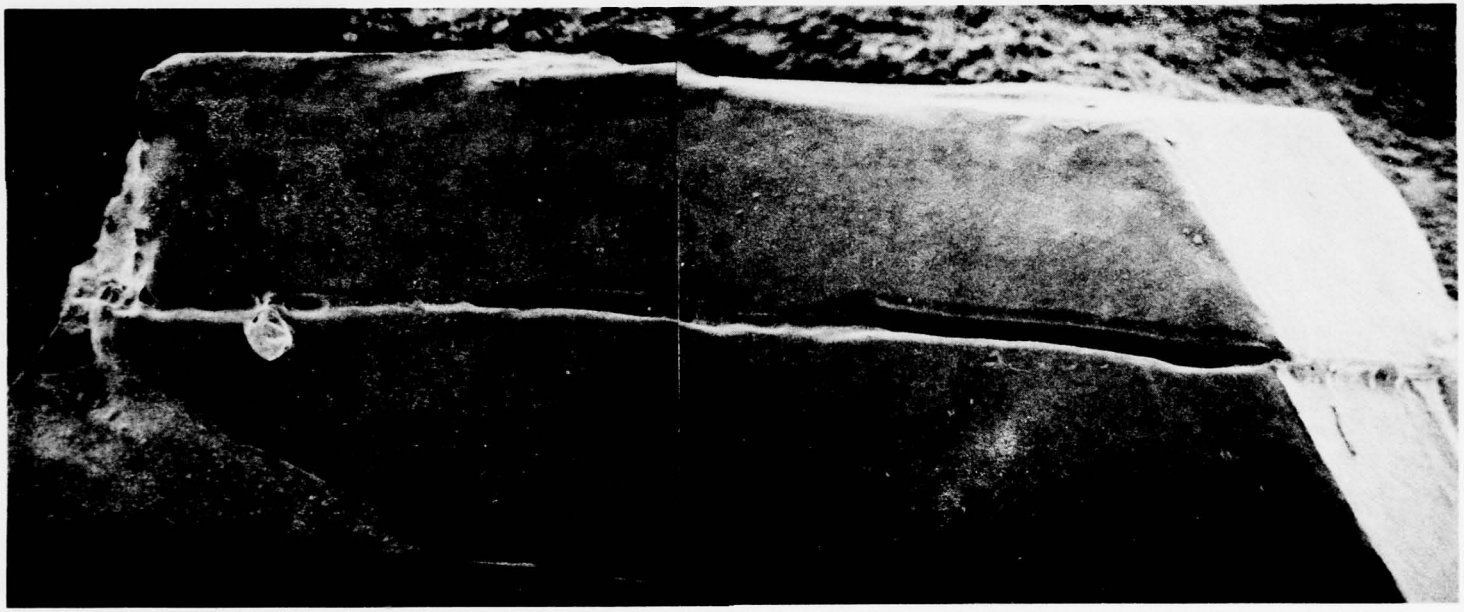

FIGURE 6-3(A)

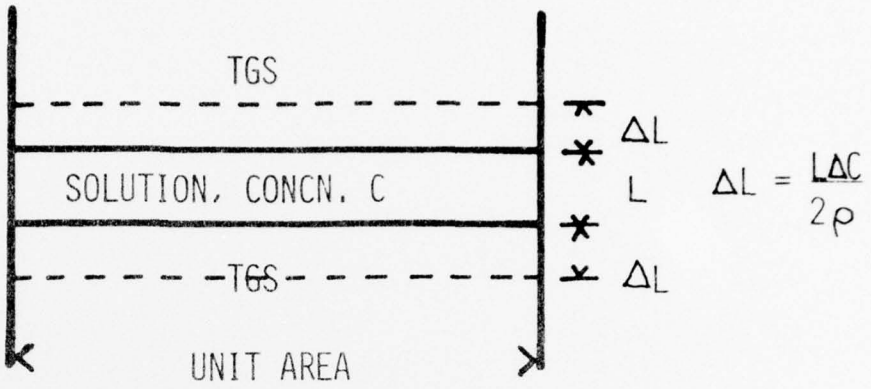


FIGURE 6-3(B) (FROM REFERENCE 6-4)

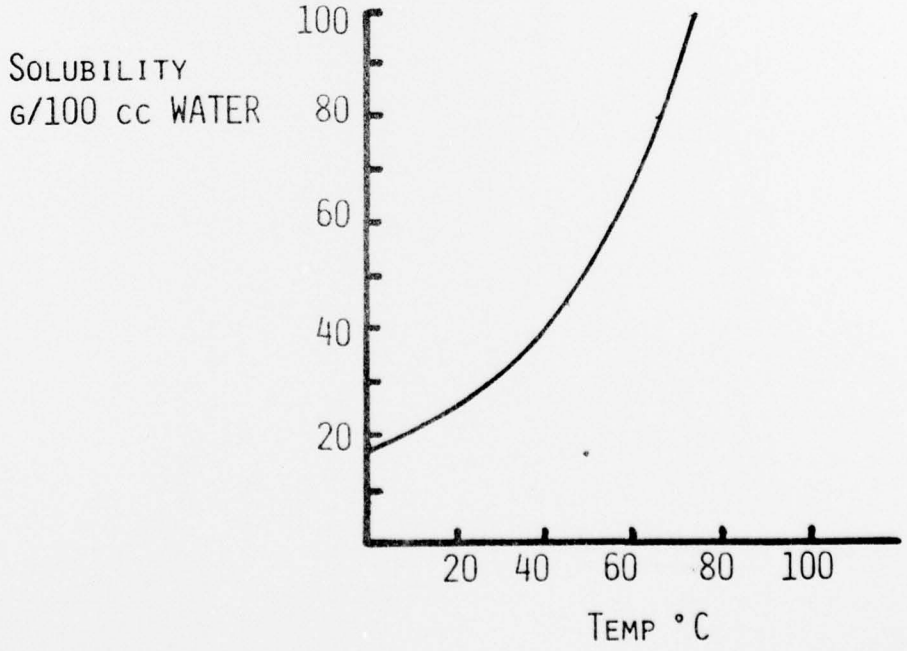

where $\Delta L$ is the thickness of TGS crystal removed by etching, $\Delta C$ is the change in TGS solution concentration, L is the initial solution thickness and $\rho$ is the density of TGS. $\Delta L$ can be increased by raising L (which can be accomplished by making the upper crystal as thin as possible to minimize pressure during bonding), or by raising $\Delta C$.

Figure 6.3b shows the increase in TGS solubility with solution temperature. The graph indicates that raising the growth temperature of the bicrystal would permit the maximum room temperature solution concentration, and yet give high $\Delta C$, and hence $\Delta L$, on heating. At equilibrium the quantity of TGS in solution between the crystals would be greatly increased compared to the room temperature concentration, and a larger bonded area would result on desiccation. According to Fig. 6.3b the growth temperature must be as high as possible to obtain maximum concentration change. However, there is some evidence[6.3] that TGS decomposes slowly above 60°C and therefore this temperature probably represents the practical upper limit. Experiments to test some of these ideas are at present in progress.

### 6.2.3 Characterization of Real and Artificial Grain Boundaries

In order to ascertain the types of boundaries which are geing generated so as to be able to compare them with the appropriate class of ceramic grain boundaries in polycrystalline samples, it is necessary to have the capability to examine the boundary region on an atomic scale. Transmission electron microscopy is the only technique capable of providing the resolution required.

To facilitate these studies a cooperative program has been initiated with the Department of Materials Science at the University of Virginia in Charlottesville. The Department in Virginia has excellent transmission microscope facilities under the direction of the Department Chairman, Dr. K. Lawless, and is

concerned with developing a regional center of excellence in this area.

To initiate cooperation, a study of the grain boundaries in PZT ceramics was begun in October 1978, centered on the question of domain wall continuity through the rather broad second-phase boundary material which is evident in SEM studies of this composition.

We believe that the commonality of interests between the faculty in Virginia who wish to work more in the ceramic systems, and have the tools and expertise for excellent transmission work, and from our own understanding of the electroceramic problems and urgent need for the high-resolution studies, an excellent joint program can be carried forward.

6.3 References

6.1 Proposal

6.2 W.D. Kingery. J. Appl. Phys. 30, 301, 1959.

6.3 B. Brezina. Mat. Res. Bull. 6, 401-412, 1971.

6.4 V.P. Konstantinova, I.M. Sil'vestrova and K.S. Aleksandrov. Sov. Phys. Cryst. 4, 63-67, 1959.

# 7. PHENOMENOLOGICAL STUDIES

## 7.1 Introduction

In simple proper ferroelectric crystals, Landau:Devonshire:Ginsburgh phenomenological theory provides a simple framework which allows the thermodynamic interrelations between elastic, dielectric, and thermal properties of the ferroelectric species accessible from any paraelectric prototype structure to be related to the first and higher order stiffnesses and coupling parameters of the prototype. From the Taylor series expansion of the free energy the first partial derivatives can be used to determine possible stable ferroic species, while the second partial derivatives interrelate the properties of species and prototype. Unfortunately, however, the sixth order polynomial forms which are required to describe the weak first order transitions characteristic of many ferroic species lead to rather cumbersome polynomial equations which become very tedious to explore, both for phase stability and property tensors.

When considering the fact that many ferroelectrics of practical interest are selected from solid solutions of end member components which are proper ferroelectrics, and that in a solid solution family, the coefficients in the expansion of the free energy mutate only slowly and continuously with composition change, it is evident that if the mathematical manipulation could be automated, the phenomenological approach could provide an effective systematic manner for interpolating in the exploratory phase diagrams for new complex multicomponent solid solution systems and for predicting the single domain properties of the ferroic species and their changes with changing elastic, dielectric and thermal boundary conditions.

Over the past three years, we have expended a considerable effort to explore computational techniques whereby the tedium of the method could be reduced and thus its potential utility enhanced. Using the ADAGE computer

graphics system at PEnn State, programming has been developed for the Devonshire form of the elastic Gibbs function for the perovskite structure ferroelectrics whose prototype is in point group m3m. The ADAGE which is a mixed analog digital system has been set up so that the dielectric stiffness and higher order stiffness coefficients and their temperature coefficients are under dial control. For any choice of these coefficients, the program will map the energies of possible stable states as a function of temperature, and calculate polarizations and permittivities in the resulting possible stable species.

To aid in the exploration of solid solutions, coefficients which reproduce the stable phases and properties of the end members can be set up, then the machine can be arranged to increment the coefficients between these end member values plotting both $\Delta G$:T and effective phase composition vs T diagrams.

The focus of this work has been to develop an energy function which would describe the single domain properties of all simple ferroelectrics in the pure $PbZrO_3$:$PbTiO_3$ solid solution system, and this task is now virtually completed. The chosen function reproduces the unusual feature of morphotropy between tetragonal and rhombohedral phases, reproduces the observed spontaneous strains from realistic values of the electrostriction constants which are almost independent of composition, gives reasonable predictions of the single domain dielectric and piezoelectric constants and magnitudes of the free energies in the different phases which agree well with those derived from thermal measurements.

## 7.2 Foci of Present Phenomenological Studies

### 7.2.1 Perovskite Ferroelectrics

(a) Using the coefficients determined in the earlier study for compositions very close to the morphotropic boundary, the effects of changing the elastic boundary conditions are being explored.

(b) For these morphotropic compositions the polarization surfaces of constant elastic Gibbs free energy are being determined as a function of temperature and of composition. The objective of this study is to determine the trajectory of the polarization which gives the lowest energy switching from rhombohedral to tetragonal states.

(c) Modifications of the Curie temperature and higher order stiffnesses are being studied which mimic the behavior of the PLZT family.

7.2.2 Tungsten Bronze and Bismuth Oxide Layer Structures

For the very large families of tungsten bronze and bismuth oxide layer structure ferroelectrics, the prototype symmetry is 4/mmm. In both families, it appears that there are simple proper ferroelectrics and also improper ferroic species. Thus the elastic Gibbs function is necessarily more complex. Formally it may be expressed in the following manner:

$$\Delta G = \Phi_1 (\eta\rho) + \Phi_2(XP) + \Phi_3(XP\eta\rho)$$

where $\Phi_1$ is a function of the independent components $\eta\rho$ of the order parameters which characterize the improper ferroic phase.

$\Phi_2$ contains the contributions related to the elastic, dielectric, and elasto-electric (electrostrictive) energies of the crystal.

$\Phi_3$ represents the coupling between the order parameters for the improper coordinates and the stress and polarization components.

The form chosen for the function $\Phi_1$ will depend on the nature of the improper phases displayed by the system. In barium sodium niobate, which exhibits an improper ferroelastic transition at 543 K, it would have the form

$$\Phi_1 = 1/2\ \alpha(\eta^2+\rho^2) + 1/4\ \beta_1(\eta^4+\rho^4) + 1/2\ \beta_2\eta^2\rho^2$$
$$+ 1/2\ \gamma_1(\eta^6+\rho^6) + 1/2\ \gamma_2\eta^2\rho^2(\eta^2+\rho^2)$$

The function $\Phi_2$ expanded to include the first sixth order terms has the general form:

$$\Phi_2 = \alpha_1^X (P_1^2+P_2^2) + \alpha_3^X P_3^2 + \alpha_{11}^X (P_1^4+P_2^4) + \alpha_{33}^X P_3^4$$

$$+ \alpha_{13}^X (P_1^2P_3^2 + P_2^2P_3^2) + \alpha_{12}^X P_1^2P_2^2 + \alpha_{333}^X P_3^6$$

$$+ \alpha_{111}^X (P_1^6+P_2^6) - 1/2\ S_{11}^P (X_1^2+X_2^2) - S_{12}^P X_1X_2$$

$$- S_{13}^P (X_1+X_2)X_3 - 1/2\ S_{33}^P X_3^2 - 1/4\ S_{44}^P (X_4^2+X_5^2)$$

$$+ Q_{13}(P_1^2X_3+P_2^2X_3) + Q_{31}(P_3^2X_1+P_3^2X_2)$$

$$+ Q_{33}P_3^2X_3 + Q_{44}(P_2P_3X_4+ P_1P_3X_5)$$

$$+ Q_{66}\ P_1P_2X_6\ .$$

The function $\Phi_3$ would again depend on the nature of the impropriety, and for barium sodium niobate the lowest order interaction terms would give

$$\Phi_3 = \theta_1\ (X_1+X_2)(\eta^2+\rho^2) + \theta_2X_3(\eta^2+\rho^2)$$

$$+ \rho_1\ (P_1^2+P_2^2)(\eta^2+\rho^2) + \rho_2\ P_3^2\ (\eta^2+\rho^2)$$

$$+ \nu_1\ (X_1-X_2)(\eta^2-\rho^2) + \nu_2X_6\eta\rho$$

At any temperature the stable states of the crystal are given from the conditions

$$\frac{\partial \Delta G}{\partial \eta} = \frac{\partial \Delta G}{\partial \rho} = 0 \qquad \frac{\partial^2 \Delta G}{\partial \eta^2} = \frac{\partial^2 \Delta G}{\partial \rho^2} > 0$$

$$\frac{\partial^2 \Delta G}{\partial \eta^2} \; \frac{\partial^2 \Delta G}{\partial \rho^2} > \frac{\partial^2 \Delta G}{\partial \eta \partial \rho}$$

$$\frac{\partial \Delta G}{\partial X_1} = \frac{\partial \Delta G}{\partial P_i} = 0$$

It is expected that the coefficients $\alpha_1^X$, $\alpha_3^X$ and $\alpha$ may be strongly and linearly temperature dependent with the forms

$$\alpha_1^X = \alpha_{1(o)}^X \; (T-\theta_1)$$

$$\alpha_3^X = \alpha_{3(o)}^X \; (T-\theta_2)$$

$$\alpha = \alpha_o \; (T-\theta_3)$$

Depending on the magnitudes of $\theta_1$, $\theta_2$ and $\theta_3$ different ferroelectric and improper ferroelastic species are accessible for the system.

The present task on this program is concerned primarily with the function $\Phi_2$ and is limited to the description of simple proper ferroelectric phases. The material family of most interest is $PbNb_2O_6$, $Pb_2NaNb_5O_{15}$ and the solid solutions between $Pb_2NaNb_5O_{15}$ and $Ba_2NaNb_5O_{15}$.

Data are being assembled and the programming developed to describe this solid solution system, using the same methods applied earlier to the PZT family.

# 8. PROGRAM ORGANIZATION: PERSONNEL AND EQUIPMENT

## 8.1 Personnel

The magnitude and scope of the present effort have required a rapid build-up of personnel and equipment for the new topics of study which are being undertaken. Over this initial period we have been most fortunate to be able to draw upon the services of two distinguished visitors, K. Uchino from the Tokyo Institute of Technology, Japan, and A. Nicol from Birmingham University in England. Uchino has been responsible for the rapid assembly and testing of the new AC precision dilatometer. Nicol, who spent three months in MRL over the summer, advised upon and devised the new temperature control equipment for crystal growth, and helped initiate the PZT growth studies.

For the theoretical work on electrostriction, Professor Barsch has been joined by Dr. N. Achar. Achar has had considerable earlier experience in problems involving fundamental lattice calculations, and has worked closely with Barsch on several earlier theoretical studies.

Work on the more practical electrostrictors is being carried forward by two graduate assistants: N. Setter, who has been growing $Pb_3Nb_2MgO_9$ single crystals and studying order:disorder phenomena in complex perovskites, and S.J. Jang, who is completing studies of electrostriction in the $Pb_3MgNb_2O_9$: $PbTiO_3$ ceramic system.

Overall responsibility for all electrostriction work is with Professor Cross, who is working closely with Uchino and Barsch to coordinate experimental and theoretical approaches.

The diphasic studies under the direction of Professor Newnham have been joined by Dr. B. Hardiman, a new faculty member who has joined MRL from the A.G. Telefunken Laboratories in Hamburg. Dr. Hardiman is working with newer replication techniques to produce composites of controlled connectivity from reusable template structures. Extrusion techniques for developing alternative

PZT composites are being carried forward by Mr. K. Klicker, who has just completed his M.S. in Solid State Science.

Newnham's work on grain oriented layer structure ceramics is also assisted by Mr. M. Holmes, a graduate assistant working on a Bismuth Institute fellowship at MRL.

Crystal growth studies, which were initiated by Dr. Nicol are now being carried forward by Ms. Susan Stephenson, a full-time research aide. Susan will be the back-up person for all growth work and is cooperating with Dr. M. Brun, who is the professional crystal grower presently in residence at MRL.

Bicrystal developments are being pushed by Dr. L. Bowen, a postdoctoral fellow from Leeds University. Dr. Bowen is being assisted by Susan Stephenson in the water soluble regrowth studies. This work is supervised by Dr. J.V. Biggers.

Phenomenological work on this program is being done by Mr. A. Amin, a graduate assistant. He is cooperating closely with Dr. H. McKinstry and Dr. R. Betsch, who are developing phenomenological methods for understanding the elastic and thermal expansion properties of tungsten bronze type ferroelectrics on other program funds.

Dielectric and piezoelectric measurements are coordinated for the whole program by Dr. W. Schulze, and all ceramic preparative and characterization studies are under the direction of Dr. J.V. Biggers.

## 8.2 Equipment

The major investment in new equipment has been concerned with modernization and automation of the dielectric and piezoelectric measurements. After a careful review of competing DEC and hobby-type digital equipment, it was decided to base the main control around an HP model 9825 system. Unfortunately, the delivery schedules for the new system and interface equipment were such that it was not possible to put them into operation over the first year of

the contract. All major items including the calculator, plotter, printer, programmer, and associated accessories are now scheduled for delivery and we anticipate automating our dielectric measurement capability early in the new year.

Three other major additions have been made over the previous year.

1. Major equipment required for the new AC precision dilatometer described in Section 2 have been installed.

2. The complete μ data track program control arrangement from Research Industries has been installed and is operational.

3. In cooperation with the MRL cement group under Dr. D. Roy, a Haake model RV-3 rotovisco-viscosimeter with a wide range of accessories for viscosities in the range of interest has been purchased and installed.

With the very comprehensive preparation and characterization equipment now available in the laboratory, the group is in excellent shape for the developing program. For the more detailed study of resonant devices we anticipate the need for an improved network analyzer, and this will be a major item required in the new year.

## 8.3 Advisory Committee

The first meeting of the ONR Advisory Committee for this program was held at Penn State on Wednesday, 27th September 1978. Members present were A. Glass, Bell Telephone Laboratories; H. Anderson, University of Missouri-Rolla; B. Jaffe, Vernitron Corporation, and V. Smith, Philips Laboratories (for S.K. Kurtz). Unable to attend were G. Kino, Stanford University and D. Berlincourt, Channel Products. Navy representatives at the meeting were R. Pohanka, ONR and NRL, Washington; P. Smith, NRL, Washington; C. LeBlanc, NUSC, New London, and R. Wollett, NUSC, New London. Guests present at the meeting were K. Okazaki, National Defense Academy, Tokyo; G. Taylor, Rutgers University (Editor, Ferroelectrics), and D. Buckner, Gulton Industries.

The Committee were given an overview of the new program during the morning of the 27th of September. The afternoon was spent in discussions and in exchange of information concerning the development of ferroelectrics and piezoelectrics in the USA and Japan. These proceedings have been reported separately.